Cell Biochemistry and Function

WILEY

CELL BIOCHEMISTRY & FUNCTION

RESEARCH ARTICLE

Determination of the In Vitro Cytotoxic Activities of Several Coumarin Derivatives on Neuroblastoma Cell Lines With In Silico Inhibitory Effects on CDK9, VEGFR2 and EGFR Proteins and ADME Studies

Fatih Caglar Celikezen[1] | Kamuran Sarac[1] | Ercan Seyhan[2] | Mehmet Enes Aslan[3] | Sena Oner[3] | Hasan Turkez[4]

[1]Department of Chemistry, Science and Letter Faculty, Bitlis Eren University, Bitlis, Turkiye | [2]Department of Basic Sciences, Faculty of Engineering, Hasan Kalyoncu University, Gaziantep, Turkiye | [3]Department of Molecular Biology and Genetics, Faculty of Science, Erzurum Technical University, Erzurum, Turkey | [4]Department of Medical Biology, Faculty of Medicine, Atatürk University, Erzurum, Turkiye

Correspondence: Ercan Seyhan (ercan.seyhan@hku.edu.tr)

Received: 29 June 2025 | **Revised:** 10 September 2025 | **Accepted:** 26 September 2025

Keywords: ADME | anticancer | coumarin | cytotoxicity | molecular docking | neuroblastoma

ABSTRACT

Due to their stable nature and medical applicability properties, coumarin derivatives have fascinated medicinal chemists in the discovery of novel therapeutics. In this study, the cytotoxic/anticancer properties of some newly synthesized coumarin derivatives were aimed at designing, synthesizing, and examining cultured human neuroblastoma cells. Moreover, molecular docking studies were carried out to determine the potential mechanism. In addition, ADMET properties were evaluated to examine the drug-likeness of newly designed coumarin derivatives. To detect the cytotoxic action of compounds, 3-(4,5-dimethylthiazol-2-yl)-2,5 2,5-diphenyltetrazolium bromide (MTT) and lactate dehydrogenase (LDH) release assays were carried out. In addition, Hoechst 33258 staining was used to detect abnormal nuclear structures. In silico, the estimates for all compounds (3a-3c) used in the study revealed that they possessed desirable physicochemical properties for bioavailability. The results of our study showed that all tested compounds exhibited remarkable cytotoxic effects on human neuroblastoma cell lines ($p < 0.05$). Additionally, among the compounds tested, **3a** and **3c** showed selective effects on neuroblastoma cells effectively at all tested concentrations. However, it was found that the selective feature of **3b**, unlike the others, was concentration-dependent. Our findings clearly showed that novel coumarin derivatives exerted potent and selective anticancer effects. Results of molecular docking studies were in parallel with in vitro studies. Unlike the majority of hybrid coumarin derivatives reported in anticancer research, the present study introduces minimalist, heteroatom-free coumarins bearing bulky aliphatic substituents. These compounds demonstrated selective cytotoxicity against SH-SY5Y neuroblastoma cells and a favorable multi-target binding profile, highlighting a distinct hydrophobic volume-based SAR. As a result, the obtained data exhibited that all used molecules may be good multitarget drug alternatives for the treatment of neuroblastoma.

1 | Introduction

Cancer is a significant disease, responsible for the deaths of an estimated 9.6 million people in 2018, according to the WHO [1]. Neuroblastoma is a neoplasm that develops from embryonic neural crest cells and is responsible for approximately 9%–15% of pediatric cancer deaths [2, 3]. Despite significant advances in treatment modalities, 5-year survival rates are still below 50% [4]. Currently, therapies including a combination of surgical resection, immunotherapy, stem cell transplantation, radiation,

Summary

- Remarkable cytotoxic effects on human neuroblastoma cell lines are determined ($p < 0.05$), and novel coumarin derivatives exerted potent and selective anticancer effects. Infrared behavior and charge transfers were compared.
- Orbital contributions of **3a-b-c** molecules play a complete role in charge transfer.
- All of the employed compounds may be suitable multitarget medication substitutes for the treatment of neuroblastoma, according to the data collected.

and chemotherapy are applied according to the risk group of the patients [5]. Serious side effects due to toxicity by chemotherapeutics in normal cells continue to be an essential obstacle in the use of chemotherapeutic drugs in clinical practice [6]. Moreover, today, traditional methods such as surgery, chemotherapy, and radiotherapy are widely used in cancer treatment. However, these methods can damage healthy cells [7]. In addition, chemotherapy drugs in use lose their effectiveness daily due to the resistance of cancer cells [8]. Many scientists worldwide have made great efforts to discover effective cancer agents with high activity and minimal adverse effects [9]. The selectivity of newly synthesized anticancer agents may bring different perspectives to the development of the drug [10].

Synthetic chemistry has a vital role in discovering new anticancer agents. The newly improved synthetic chemistry methods expedite the novel drug discovery and development process, including small molecules [11, 12]. Moreover, synthetic chemistry makes it easier to research effective interactions that kill cancer cells selectively while protecting healthy cells [13]. At this point, coumarin derivatives, natural or synthetic, gained importance as promising scaffolds for drug discovery because of their biological activities and structural simplicity [14].

Coumarins, naturally occurring in higher plants, are phytochemicals in the polyphenol class with some medicinal properties. Coumarins belong to the benzopyrone class. They represent an essential resource for discovering novel anticancer agents [15, 16]. In addition, medicinal chemists have been attracted to the discovery of coumarin derivatives because of their stability, solubility, and medical properties [17, 18]. Anticancer effects of coumarin derivatives in human cervical cancer cell lines have been reported in recent studies by Maleki et al. [19], Hybrid lonidamine-coumarin derivatives were also shown to have anticancer activity by Ipek et al. [20]. In another study, the anticancer potential of novel dipyrromethane-coumarin and porphyrin-coumarin derivatives was highlighted by Holiyachi et al. [21]. Most reported anticancer coumarins are hybrid scaffolds bearing heteroatom-rich linkers or secondary pharmacophores targeting kinases such as EGFR and VEGFR-2. However, studies focusing on minimalist, heteroatom-free coumarins with activity against neuroblastoma cells remain rare [22, 23].

In addition, the FDA (US Food and Drug Administration) does not approve a compound even if it has good biological activity due to its absorption, distribution, metabolism, excretion, and toxicity (ADMET) properties or adverse side effects [24]. Therefore, in silico modeling and ADMET estimation for effective drug development have also attracted the attention of researchers. The fact that these methods are accessible and

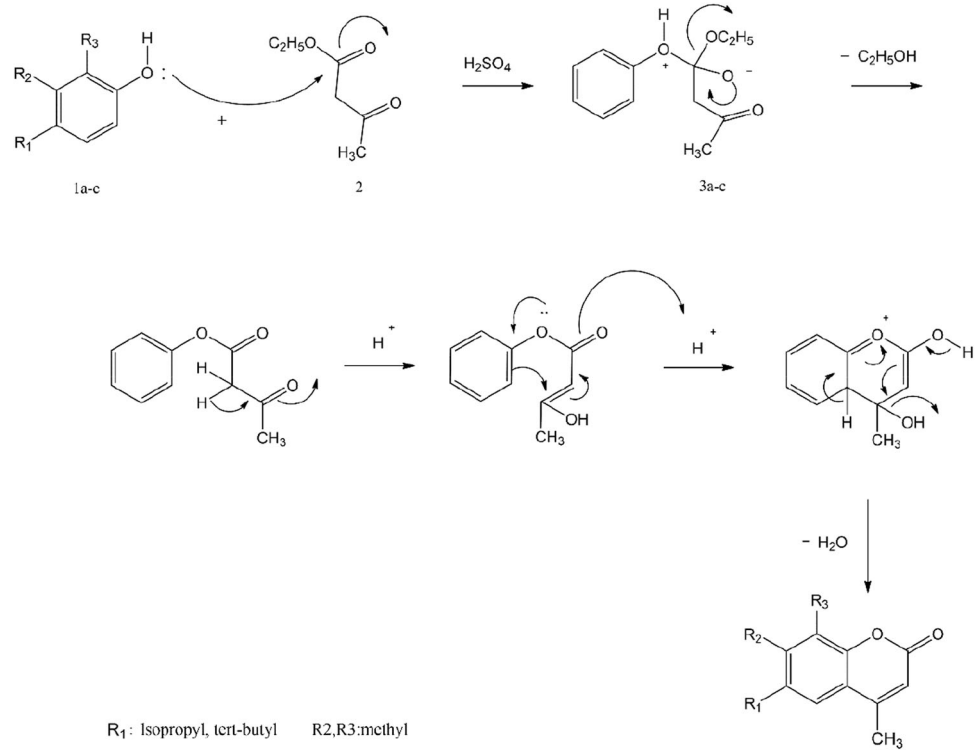

FIGURE 1 | Mechanism and the structures of novel coumarin derivatives.

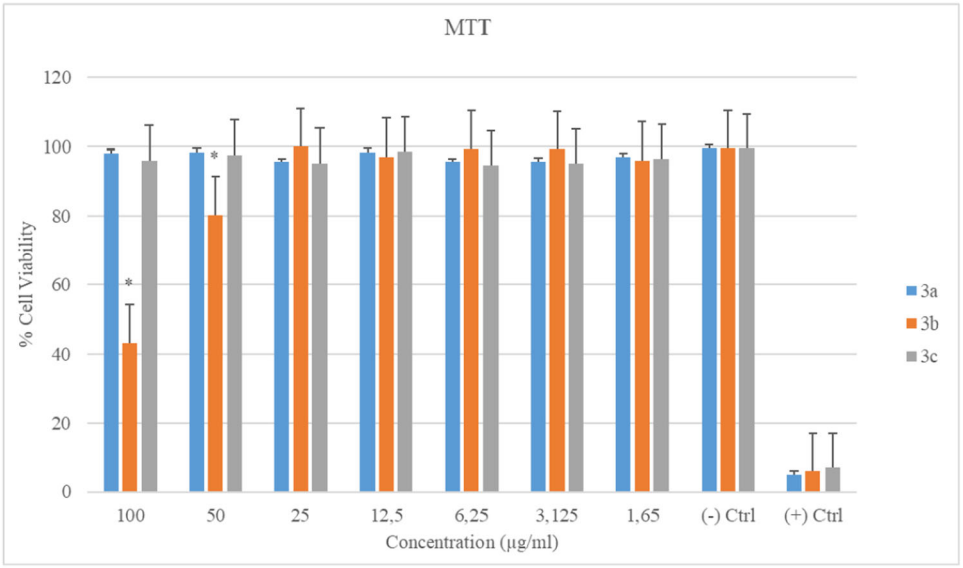

FIGURE 2 | MTT analyses of the HDFa cell lines treated with novel derivatives for 24 h. (*) Symbols indicate a statistically significant reduction vs. the negative control.

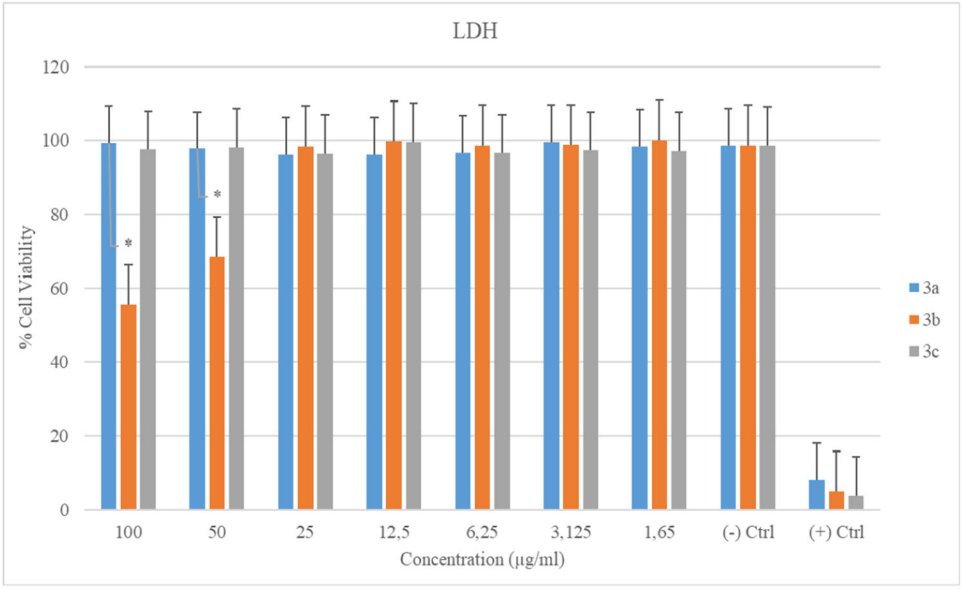

FIGURE 3 | Cell viability tests of the HDFa cell lines treated with novel derivatives for 24 h. (*) Symbols indicate statistically significant reduction vs. the negative control.

easy, that the biological activities of newly designed molecules can be predicted based on structure, or that safety, bioavailability, and activity can be analyzed in parallel, reveals a more effective drug development process [25]. Moreover, molecular docking studies have been widely used by many researchers recently. The most important feature of these studies is the determination of protein-ligand interactions using in silico methods [26–28].

On the other hand, targeting specific proteins in cancer treatment is an increasing trend in new anticancer drug development [29]. EGFR (epidermal growth factor receptor), VEGFR-2 (vascular endothelial growth factor receptors), and CDK9 (Cyclin-dependent kinase-9) are the specific proteins in cancer treatment, including neuroblastoma SH SY5Y cell lines [30–32]. Targeting dual inhibition of EGFR and VEGFR2 proteins, which have a vital role in tumor growth and angiogenesis, is a promising approach for cancer treatment [33, 34]. Moreover, targeting the CDK9 receptor, which is an essential regulator of transcription, in cancer treatment is also a promising strategy. Today, CDK9 inhibitors exhibit an essential potential for cancer treatment, and some inhibitors of this protein are in clinical trials [35]. EGFR supports growth, proliferation, differentiation, and survival signaling of mammalian cells [36]. It has been reported that EGFR's widespread expression is available in neuroblastoma tissue

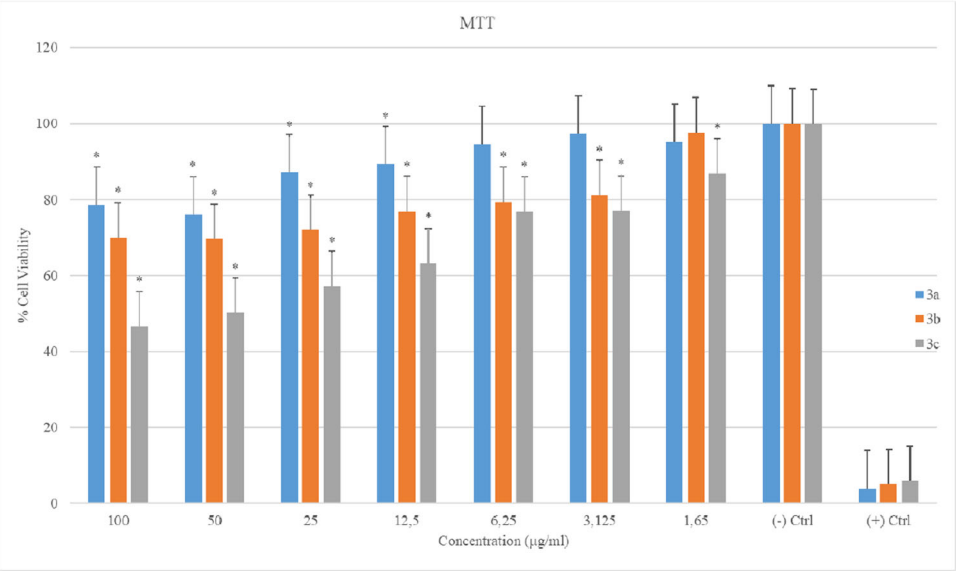

FIGURE 4 | MTT analyses of SH-SY5Y cell lines treated with novel derivatives for 24 h. (*) Symbols indicate statistically significant reduction vs. negative control.

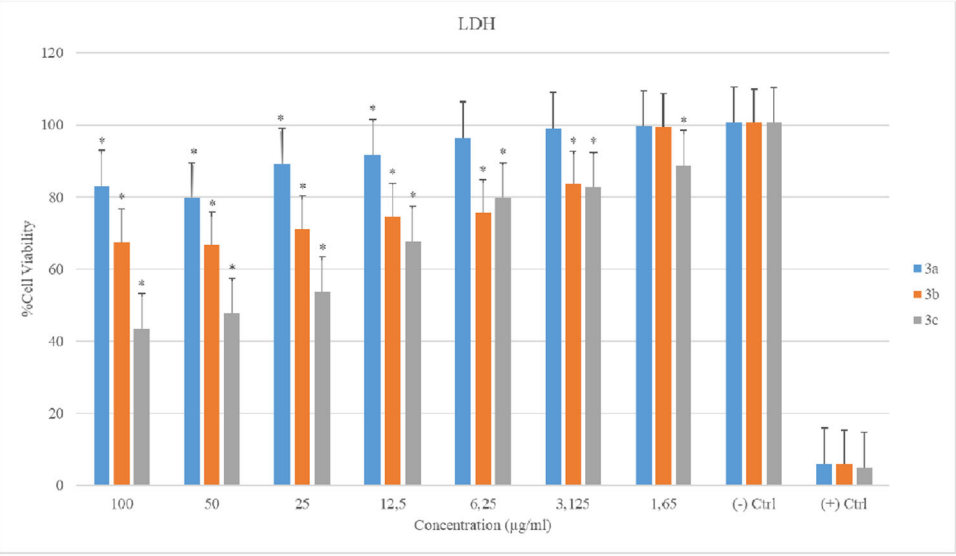

FIGURE 5 | Cell viability analyses of SH-SY5Y cell lines treated with novel derivatives for 24 h. (*) Symbols indicate a statistically significant reduction vs. the negative control.

and cell lines. This makes EGFR an attractive target for new therapies [37, 38]. The VEGFR protein has the ability to control the cellular proliferation of cancer cells, including neuroblastoma [39, 40]. Next, CDK9 proteins are regulators for RNA transcription of Mcl-1 proteins in the neuroblastoma SH-SY5Y cell line. It has been reported that the inhibition of RNA synthesis, which is related to CDK9 blocking, suggests that it may inhibit the growth of neuroblastoma cell lines [41].

The goal of the research was to design, synthesize, and determine the biological activity of some novel coumarin derivatives on human neuroblastoma cell lines, considering the problems arising from the lack of selectivity and specificity encountered in cancer treatment, and to evaluate in silico interactions of synthesized molecules and CDK9, EGFR, and VEGFR2 via the molecular docking method. In addition, the ADME properties of molecules were determined.

2 | Materials and Methods

2.1 | General Procedure for the Synthesis of 3a-c

Substituted phenol (**3a–c**) and ethyl acetoacetate (0.01 mol), sulfuric acid (50 mL) mixture was refluxed for 2 h. Solid coumarin formed in the reaction flask after 4 h, and then the reaction ended. The obtained residue was mixed with ice by stirring. It was filtered, dried, and recrystallized using ethyl alcohol. In addition, ^{1}H-NMR and ^{13}C-NMR graphics of

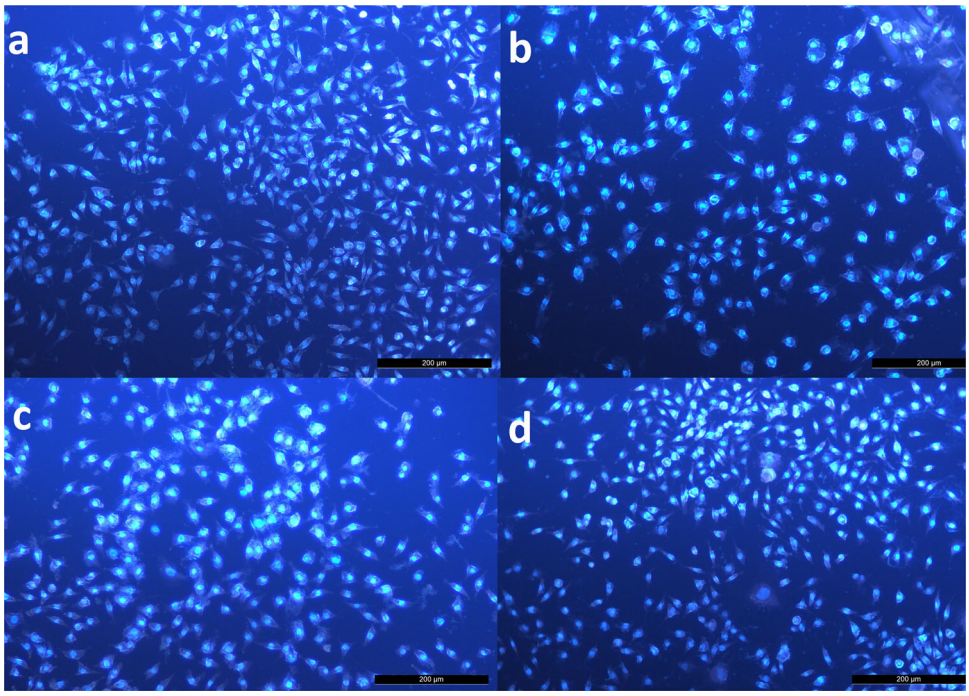

FIGURE 6 | Hoechst 33258 fluorescent staining of HDFa cell cultures. (a) Negative control (no administration), (b) 100 μg/mL of **3b** administration, (c) 100 μg/mL of **3c** administration, and (d) 100 μg/mL of **3a** administration to the HDFa cell cultures.

TABLE 1 | Nuclear aberrations (NA) in the fibroblast cell line (HDFa) in response to compounds applied at a concentration of 100 μg/mL. Readings are mean ± SEM of 3 samples per 1000 cells. The statistical differences in the same column were shown with different letters. The application values were calculated for 24 h period (GraphPad Prism 7, ANOVA: Significant differences in samples were calculated by Dunnett's multiple comparison test).

Nuclear abnormalities (NA)				
Treatment	**Total MN**	**Total lobbed**	**Total notched**	**Mean NA/1000 cells ± SD**
(−) Ctrl	7	8	8	0.023 ± 0.005a
3a	5	8	9	0.022 ± 0.002a
3b	8	5	11	0.024 ± 0.003a
3c	9	6	8	0.023 ± 0.002a

the compounds are given in Supporting Information S1: Figures S1–S6.

In this study, new derivatives of coumarin class compounds were synthesized. The reaction to form the coumarin ring took place via the von Pechmann condensation mechanism. In this reaction, substituted phenols were reacted with ethyl acetoacetate under sulfuric acid catalysis to obtain substituted 4-methylcoumarin. The reaction mechanisms of the synthesized compounds are shown in Figure 1.

2.2 | Chemical Assays

IR spectra were measured using a Perkin-Elmer Spectrum One FT-IR spectrophotometer. NMR was performed on a Bruker AC-400 NMR spectrometer at 400 MHz for 1H and 100 MHz for 13 C. The compounds were dissolved in DMSO, and the chemical shifts were determined with respect to TMS (for 1H and 13 C NMR). The chemicals were purchased from Sigma-Aldrich (Taufkirchen, Germany) and Merck (Darmstadt, Germany), respectively.

2.3 | Biological Assays

2.3.1 | Cell Cultures

The human fibroblast cell line (HDFa, ATCC PCS-201-012) was grown in DMEM medium including 1% penicillin/streptomycin antibiotic mixture and fetal bovine serum (FBS, 10%) at 37°C temperature with 5% CO_2 until it reached 80% confluency. Neuroblastoma cell line (SH-SY5Y, ATCC CRL-2266) was grown by using 1% penicillin/streptomycin, and FBS (10%) in DMEM/F12 culture media. When the medium was brought to 37°C, 5 mL was transferred in a T25 flask. SHSY-5Y cells were cultivated at 37°C with 5% CO_2 level. Cells in the flask were incubated until they reached 80% density.

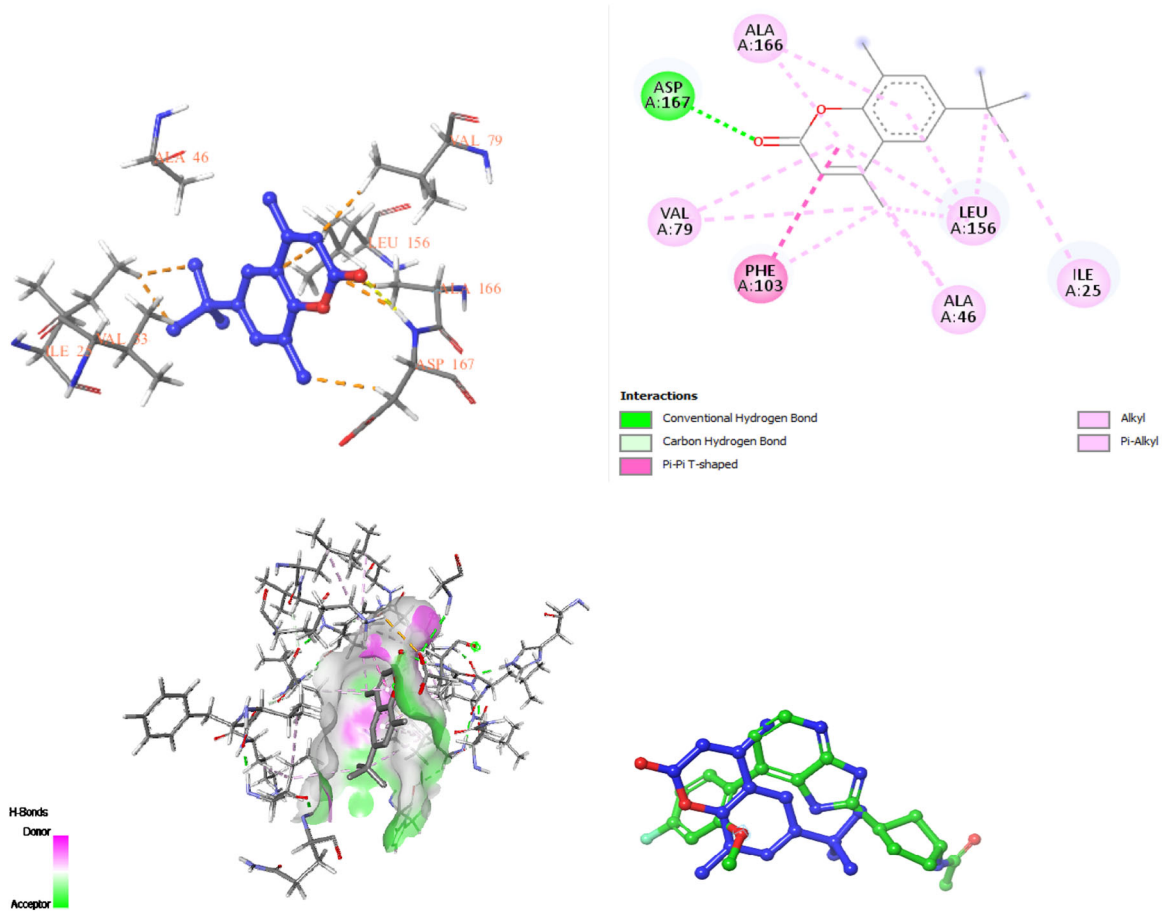

FIGURE 7 | The visualisation of the interactions of **3a** and CDK9, 3D, 2D, Hydrogen bonds and superimpose of **3a** and reference ligand UT5.

TABLE 2 | Molecular docking scores of used molecules.

	Target Proteins		
Molecule	**CDK9 ΔG (kcal/mol)**	**VEGFR2 ΔG (kcal/mol)**	**EGFR ΔG (kcal/mol)**
3a	−8.1	−8.9	−7.1
3b	−7.8	−8.3	−6.3
3c	−8.1	−8.6	−6.8
UT5	−10	—	—
D0D			−8.6
42Q		−13.3	

2.3.2 | Cell Viability and Cytotoxicity Analyses

The cell death rate of the cell cultures was analyzed using the LDH assay (Cayman Chemical Company, USA), following the instructions of the manufacturer. A 96-well plate was seeded with cell cultures. Compounds at various concentrations (1.65 to 100 μg/mL) were applied to cultures for 24 h. After incubation, 100 μL culture supernatant was discarded into a fresh 96-well plate. Then, 100 μL reaction mixture was added, and the color intensity was observed at 490 nm absorbance. The samples were incubated at room temperature for 30 min. The absorbance was monitored using a microplate reader at 490 nm. 3-(4,5-dimethylthiazol-2-yl)-2,5-diphenyltetrazolium bromide (MTT) assays were used to determine the viability of the fibroblast and neuroblastoma cell cultures. The doses ranged from 1.65 μg/mL to 100 μg/mL, and the incubation time was 24 h. Ten microlitres of MTT solution was then added to each well, and incubation was allowed at 37°C for 3 h. The cell medium was discarded. Hundred microlitres of DMSO was added to each well to dissolve the crystals and give them a blue color. The color intensities were measured using a microplate reader at a wavelength of 570 nm.

2.3.3 | Hoechst 33258 Fluorescent Staining and Nuclear Abnormality Analysis

The abnormal nuclear structures were detected by Hoechst 33258. To monitor nuclear morphology, the compounds were applied to fibroblast cultures at concentrations of 100 μg/mL, and the cultures were incubated for 24 h. Phosphate-buffered saline containing 4% paraformaldehyde was used. Cells were fixed for 30 min at 4°C. The cell cultures were washed twice with PBS and then incubated with 1 μM of the fluorescent dye Hoechst 33258 for 5 min at room temperature. Fluorescence microscopy was used to photograph the observed cells (Leica DM IL LED).

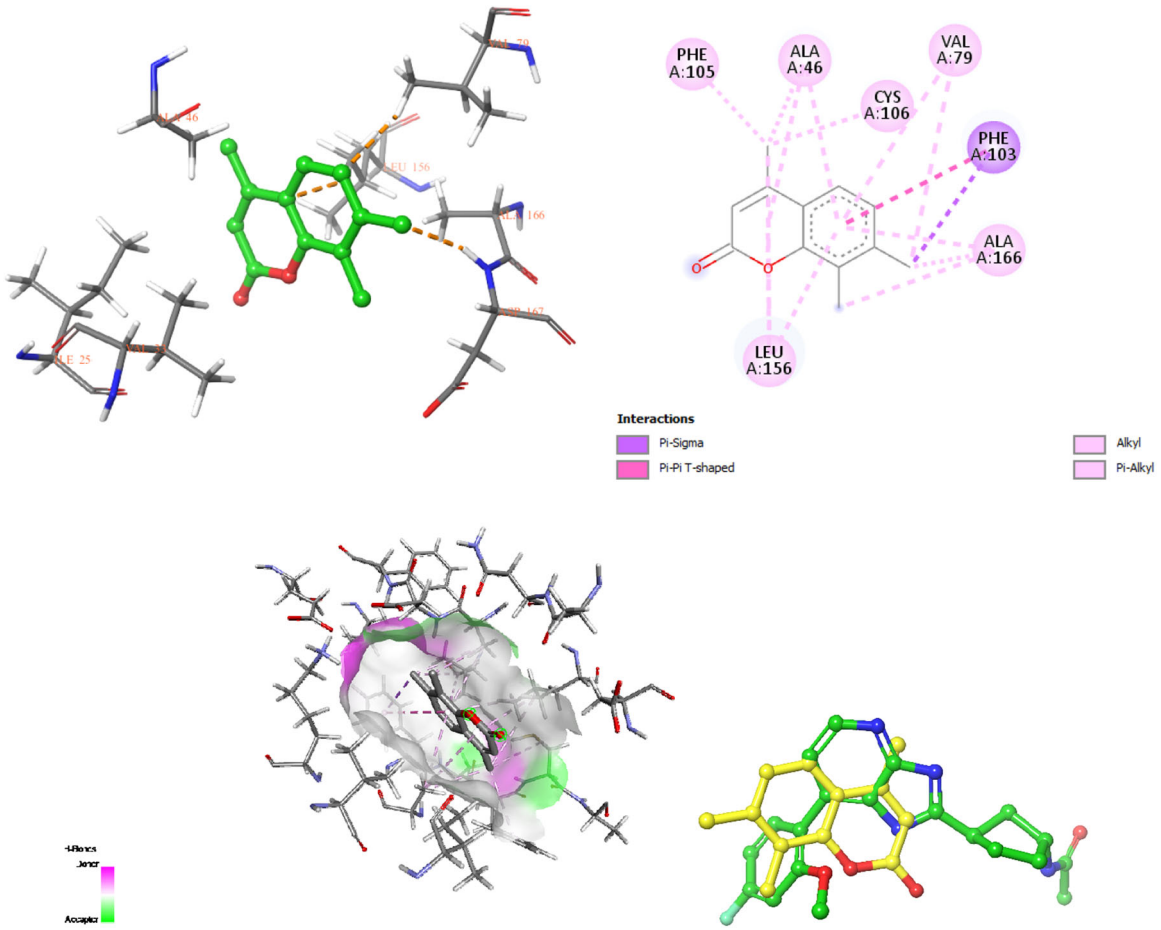

FIGURE 8 | The visualisation of the interactions of **3b** and CDK9, 3D, 2D, Hydrogen bonds and superimpose of **3b** and reference ligand UT5.

2.4 | In Silico Studies

2.4.1 | Molecular Docking

The Autodock Vina program was used to calculate the binding affinity of the synthesized coumarin compounds. To obtain the 3D structures of the compounds and to perform the geometry optimization, the Avogadro 1.2.0n package program was used. The optimized structures were recorded in *.mol2 format. The X-ray crystal structures of CDK9, VEGFR2, and EGFR (PDB ID: 7NWK, resolution: 2.81 Å, PDB ID: 3VHE, resolution: 1.55 Å, and PDB ID: 8SC7, resolution:1.98 Å, respectively) of the proteins obtained from the protein data bank website [http://www.rcsb.org/pdb]. Proteins downloaded in *.pdb format. The protein structures were optimized using the Maestro viewer within the Schrödinger program. The files are recorded in *.pdb format. To visualize 3D and 2D structures, PyMOL and Biovia Discovery 2024 Client programs were used. For the validation of docking studies, we extracted ligands from the X-ray structures of proteins and re-docked them. We then presented the superimposed modes of the synthesized ligands. Then the Maestro viewer Schrödinger program was used to calculate RMSD values.

2.4.2 | ADME Prediction

Many chemical compounds synthesized to obtain drug-active ingredients fail due to their low bioavailability profiles. Therefore, in silico ADMET scores are evaluated, making them an important part of drug discovery research. These studies reduce the likelihood of any drug candidate failing in clinical trials. The in silico-toxic properties of the synthesized compounds were evaluated using a Protox-II free web server [42]. In silico pharmacokinetic properties are also predicted via the SwissADME free web tool [43]. The prediction of brain penetration and gastrointestinal absorption was studied with the BOILED-Egg model [44].

2.5 | Statistical Analyses

The GraphPad Prism (GraphPad Software, Version 8, San Diego, USA) statistical program was used for statistical evaluations. One-way ANOVA and Dunnett comparison tests were used. The level of statistical significance was accepted as $p < 0.05$.

3 | Results

Synthesis of 6-tert-butyl-4,8-dimethyl coumarin (**3a**) ($C_{15}H_{18}O_2$) White solid, yield 40%, m.p. 157°C–159°C; FT-IR (KBr, cm−1, υ): 3000–3100 (Ar−H), 2880–2989 (C−H), 1710 (C=O, lactone), 1587(C=C, Ar), 1147(C−O−C, Lactone); ^{1}H-NMR (400 MHz, DMSO-d6, δ, ppm): 1.35 (s, 9H (CH3)3C), 2,50 (s, 6H) CH3; 6,30 (s, 1H) (lactone); 7,45 (s, 2H) (Ar). ^{13}C-NMR (100 MHz, DMSO-

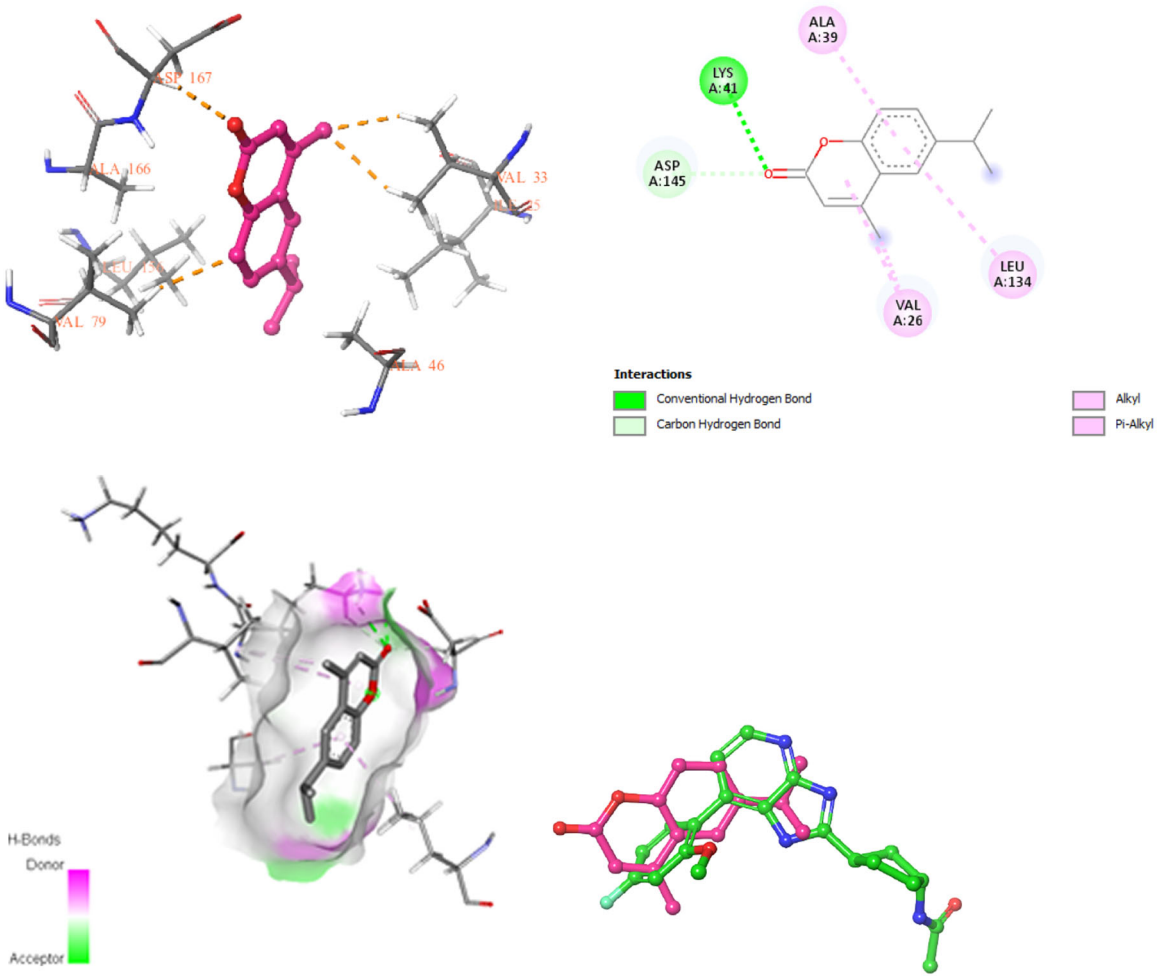

FIGURE 9 | The visualisation of the interactions of **3c** and CDK9, 3D, 2D, Hydrogen bonds and superimpose of **3c** and reference ligand UT5.

d6, δ, ppm): 16, 19, 32, 35, 112, 120, 121, 124, 125, 142, 145, 153, 160. Among these values, structures between 0 and 50 ppm indicate the presence of CH_3, which reduces the ability to attract bond electrons. The effect of the fourth bond, the C─C structure, is seen at values of 16, 19, 32, and 35 ppm. However, there are 5 CH_3 and 1 tert C─C bond, emphasizing the C─C structure. It has a high density at 32 ppm (two times the NMR density at 16 ppm) (Supporting Information S1: Figures 1–6). There is also a similarly high NMR density of 35 ppm. So there are two overlaps here. It overlapped the carbon atom in the CH_3 molecules, which directly binds to the aromatic ring, exhibiting a strong, similar chemical environment at 32 ppm. Sixteen ppm represents one of the CH_3s in 6-tert-butyl. Nineteen ppm indicates the central C atom in the tert-structure. Thirty-five ppm represents the two carbon atoms in CH_3 that are symmetrical to each other in the tert-structure. The C═O structure, which has the highest electronegative properties, is responsible for 160 ppm. The structure at 153 ppm is responsible for a low electronegativity (C─O) bond. The remaining 7 ppm values (112, 120, 121, 124, 125, 142, 145) belong to the carbon atoms in the aromatic ring. There is no overlap in this aromatic region.

Synthesis of 4,7,8-trimethyl coumarin (**3b**) ($C_{12}H_{12}O_2$) White solid, yield 80%, m.p. 145°C–146°C; FT-IR (KBr, cm^{-1}, υ): 2980–3090 (Ar─H), 2870–2989 (C─H), 1690 (C═O, lactone), 1600(C═C, Ar), 1185(C─O─C, Lactone); ^{1}H-NMR (400 MHz, DMSO-d6, δ, ppm): 2.30 (s, 9H) CH3; 6,15 (s, 1H) (lactone); 6,90- 7,40 (m, 2H) (Ar). ^{13}C-NMR (100 MHz, DMSO-d6, δ, ppm): 12,19, 20, 112, 116, 123, 125, 126, 141, 150, 151, 161. Looking at Supporting Information S1: Figure S4, the values at 12, 19 and 20 ppm show the presence of 3 CH_3 structures with almost equal density. The fact that their chemical shift values are close to each other and their peak intensities are practically equal to each other shows that they have a similar bonding structure. Similar to molecule **3a**; The C═O structure, which has the highest electronegative properties, is responsible for 161 ppm. The structure at 151 ppm is responsible for a low electronegativity (C─O) bond. The remaining ppm values (112, 116, 123, 125, 126, 141, and 150) indicate the presence of 7 carbons in the aromatic ring. Since these carbons do not have similar chemical structures, there is no overlap.

Synthesis of 6-isopropyl-4-methyl coumarin (**3c**) ($C_{13}H_{14}O_2$) White solid, yield 40%, m.p. 154°C–155°C; FT-IR (KBr, cm−1, υ): 2985–3110 (Ar─H), 2885–2995 (C─H), 1711 (C═O, lactone), 1625 (C═C, Ar), 1190 (C─O─C, Lactone); ^{1}H-NMR (400 MHz, DMSO-d6, δ, ppm): 1.25 (d 6H) (CH3)2; 6,25 (s, 1H) (lactone); 7, 10- 7, 55 (m, 3H) (Ar). ^{13}C-NMR (100 MHz, DMSO-d6, δ, ppm): 19, 23, 33, 115, 118, 121, 124, 130, 146, 151, 153, 161. Here, chemical shift values of 19, 23, and 33 indicate 3 CH3 groups. However, one of the peak intensities (23 ppm) is almost twice as large as the others. Here, an overlap increases the probability.

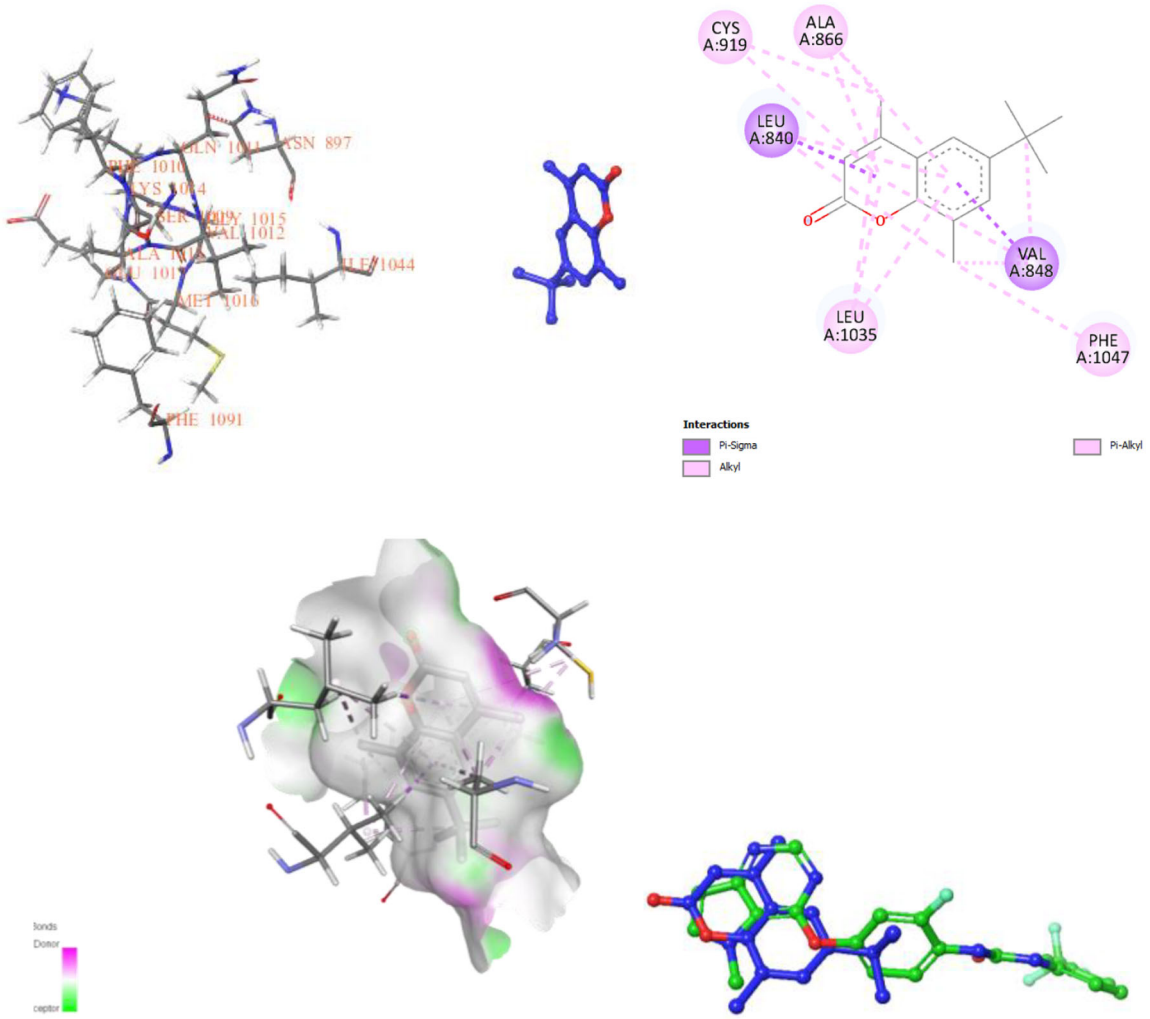

FIGURE 10 | The visualisation of the interactions of **3a** and VEGFR2, 3D, 2D, Hydrogen bonds and superimpose of **3a** and reference ligand D0D.

As in the **3a** molecule, two CH_3 groups have the same chemical environment as each other. The 6-isopropyl structure shows the appropriate structure for this situation. One of these chemical shift values represents 4-methyl I, while the other is the C─C connection in 6-isopropyl. As in molecules **3a** and **3b** described above, the C═O structure with the highest electronegative properties is responsible for 161 ppm. The structure at 153 ppm is responsible for a low electronegativity (C─O) bond. The remaining 7 ppm values are for carbonaceous structures in the aromatic ring. Here, the value of 151 ppm belongs to the carbon atom at the aromatic junction of the 6-isopropyl structure due to its high electronegative environment. In this structure, there is an overlap in the C─C structure, as in molecule **3a**.

The analysis of the infrared spectra of the aforementioned compounds reveals the presence of C─O stretch bands at 1179 cm^{-1}, 1185 cm^{-1}, and 1176 cm^{-1}, as well as aromatic C═C stretch bands at 1625 cm^{-1}. Additionally, the 1601 cm^{-1} and 1625 cm^{-1} spectra, as well as the distinct lactone carbonyl peak of coumarin at 1715 cm^{-1}, 1690 cm^{-1}, and 1711 cm^{-1}, are evident. In the 1H NMR spectra of the title compounds, the most characteristic peaks were observed in the regions corresponding to the methyl groups at the carbon atoms C-4 and C-3, the hydrogen atoms in the aromatic rings, and the proton of the substituted phenol (OH).

The (CH3) (C-4) hydrogen is observed as a singlet at 2.40, 2.30, 2.35 ppm; the (CH) (C-3) hydrogen is observed as a singlet at 6.25, 6.15, 6.25 ppm; the hydrogen in the aromatic ring is identified as a multiplet in the range of 10 to 6.90 ppm. Additionally, the proton of the substitutional phenol (OH) utilized in the starting material is not observed at 5.35, 5.34, and 5.35 ppm, respectively. In the 13 C NMR spectrum, the lactones were observed at 163, 166, and 162 ppm.

In the present study, the selective anticancer properties of newly synthesized coumarin derivatives were determined via MTT and LDH release assays. The test results showed that compounds **3a** and **3c** exhibited significant selective effects against cancer cells at all tested concentrations. Compound **3b** acted selectively at low concentrations but failed to maintain this property at high concentrations (Figures 2–5). To assess the selective cytotoxic effects of coumarin derivatives 3a–3c, IC_{50} values were determined for both human dermal fibroblast (HDFa) and neuroblastoma (SH-SY5Y) cell lines. Compounds 3a and 3b showed IC_{50} values exceeding 1000 μg/mL in HDFa cells, indicating minimal cytotoxicity toward normal fibroblasts. In contrast, compound 3c demonstrated an IC_{50} value of 146.72 μg/mL in HDFa cells. In neuroblastoma SH-SY5Y cells, all three compounds exhibited significantly lower IC_{50} values,

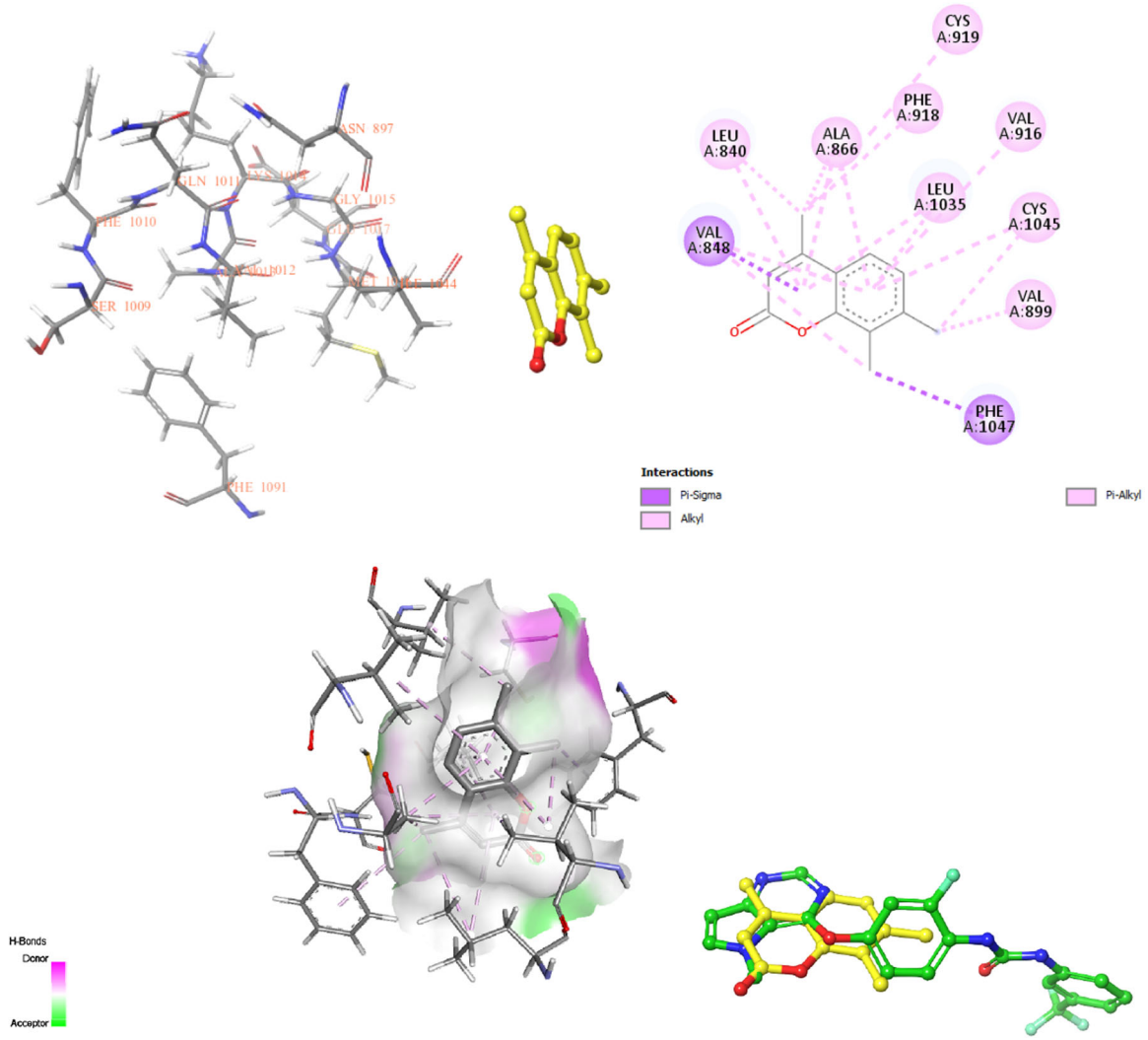

FIGURE 11 | The visualization of the interactions of **3b** and VEGFR2, 3D, 2D, Hydrogen bonds and superimpose of **3b** and reference ligand D0D.

with 3a, 3b, and 3c showing 230.54, 213.38, and 48.26 μg/mL, respectively. Based on these results, Selectivity Index (SI) values were calculated. Compounds 3a and 3b demonstrated SI values ≥ 4, while compound 3c exhibited an SI of 3.04. These results suggest that 3a and 3b possess a more favorable selectivity profile for neuroblastoma cells over normal fibroblasts. In addition, Hoechst 33258 fluorescent staining results stated that there is no significant difference in cell surface distributions and nuclear morphologies after treatment with novel derivatives (Figure 6 and Table 1).

Molecular docking studies indicated that all used molecules have good interaction potential with the receptors. And ADME analyses showed all molecules have potentially good druglike properties and powerful bioavailability features.

Molecular docking results of CDK9

Molecular docking results of VEGFR2

In addition, the pharmacokinetic properties of the title compound were predicted via several web tools. Bioavailability radar (SwissADME, Figure 17) reflects the region identified as safe, indicated by a pink hexagon, and the red lines in this area indicate the locations of the synthesized compounds. Based on this data, it can be defined as safe since the title compound is in the applicability region. The SwissADME web tool estimates the bioavailability of a drug based on five different criteria (Lipinski, Veber, Egan, Ghose, Muegge) [42].

4 | Discussion

In the field of cancer treatment, significant progress has been made. However, the management of malignancies in patients remains an important concern for modern medicine. In addition to radiotherapy and surgical treatments, cancer cases are also treated with chemicals. These treatment approaches minimize the pain caused by surgical interventions or the harmful effects of nuclear radiation [43]. Coumarins have come to the forefront with their remarkable features in this field. Natural and synthetic coumarin derivatives have gained importance with their therapeutic properties in photochemotherapy and cancer [45]. In addition, it has been shown that coumarin and coumarin compounds rarely cause nephrotoxicity, cardiotoxicity, dermal toxicity, hepatotoxicity, and other side effects [46].

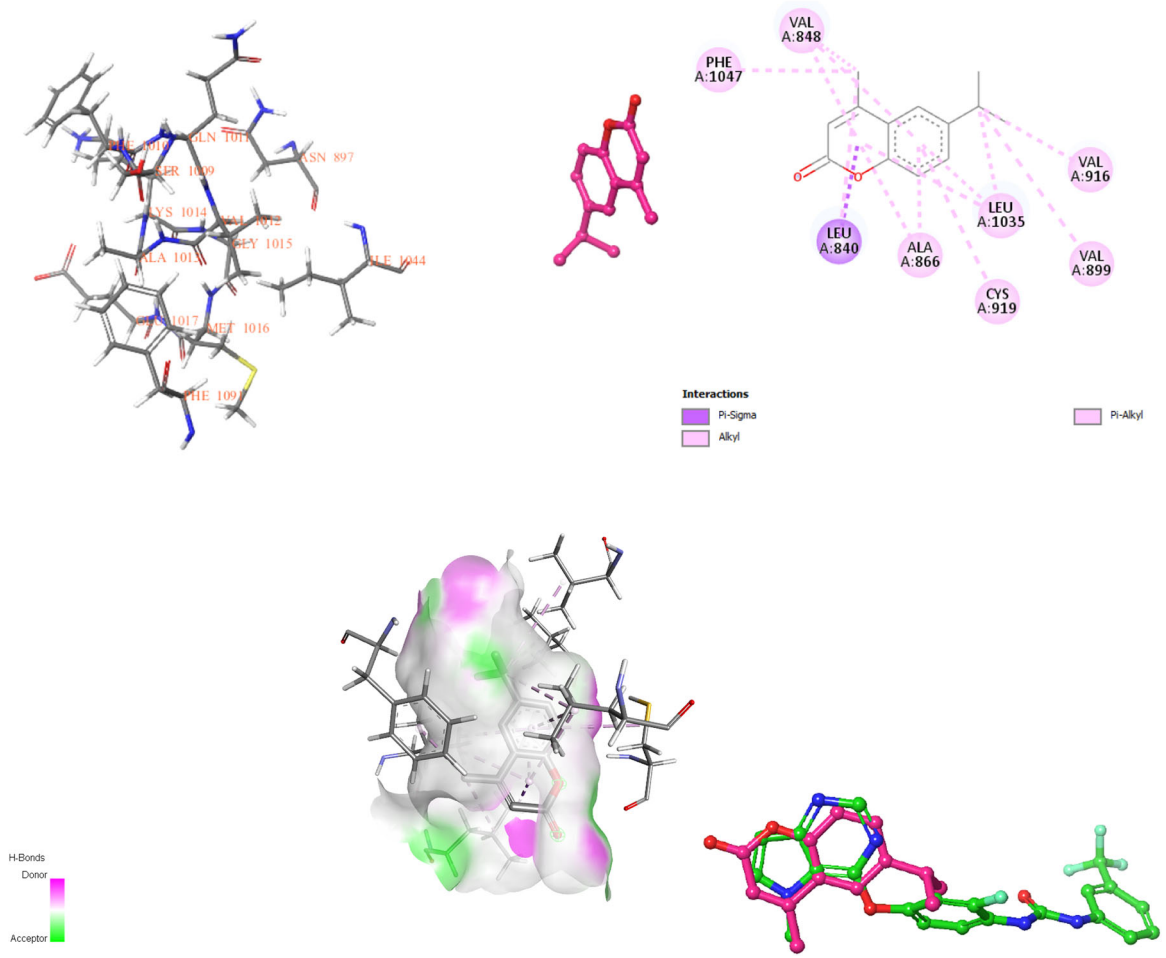

FIGURE 12 | The visualisation of the interactions of **3c** and VEGFR2, 3D, 2D, Hydrogen bonds and superimpose of **3c** and reference ligand D0D.

In the present study, the cytotoxic abilities of synthesized coumarin derivatives were evaluated on HDFa and SH-SY5Y cell lines spectrophotometrically. The obtained results indicated that only **3b** molecules showed toxic effects on HDFa cell lines at higher concentrations (50 and 100 μg/mL), and these results were statistically significant ($p < 0.05$). When the obtained results on SH-SY5Y were evaluated **3a** and **3c** molecules indicated toxic effects on SH-SY5Y cells at concentrations between 3.125 μg/mL and 100 μg/mL in statistically significant levels. Moreover, only **3c** molecule exhibited a toxic effect at a concentration of 1.65 μg/mL at a statistically significant level ($p < 0.05$). These data indicated that **3a** and **3c** presented a strong selective effect at significant statistical levels. 3b molecule has a selective effect, but only low than 50 μg/mL (Figures 2–5). The comparison of IC_{50} values between normal fibroblast (HDFa) and neuroblastoma (SH-SY5Y) cell lines revealed that compounds **3a** and **3b** exert strong selective cytotoxic effects against cancer cells, with minimal toxicity toward healthy cells. Their high Selectivity Index (≥ 4) underscores their potential as safer therapeutic candidates. Notably, compound **3a**, despite its relatively higher IC_{50} value in cancer cells, displayed the most pronounced selectivity, suggesting that it could inhibit tumor growth without significantly affecting noncancerous tissues. In contrast, compound **3c**, while more potent in SH-SY5Y cells ($IC_{50} = 48.26$ μg/mL), showed reduced selectivity due to its cytotoxicity in HDFa cells, lowering its SI to 3.04. These findings align with the overall aim of anticancer drug development, which prioritizes compounds with potent anticancer activity alongside high selectivity to minimize adverse effects on normal tissues. The selectivity profiles of these coumarin derivatives support their candidacy for further development, with **3a** and **3b** in particular offering promising potential for targeted neuroblastoma therapy. Besides, Hoechst 33258 fluorescent staining data indicated that there is no important difference in cell surface distributions and nuclear morphologies after treatment with the used molecules (Figure 6 and Table 1).

In contrast to the hybrid designs commonly described in the literature—such as coumarin–triazoles, coumarin–benzofurans, or coumarin–thiosemicarbazones—our compounds feature bulky aliphatic substituents (tert-butyl, isopropyl) at the C-6 position of the 4-methylcoumarin core and perimethylation. This minimalist and hydrophobic substitution pattern produced significant cytotoxicity in SH-SY5Y neuroblastoma cells while sparing human dermal fibroblasts.

These findings demonstrate a hydrophobic volume-based structure–activity relationship, offering an alternative to the heteroatom-driven interaction paradigms that dominate coumarin anticancer research. Moreover, the observed multi-target binding (CDK9, VEGFR-2, EGFR) without additional

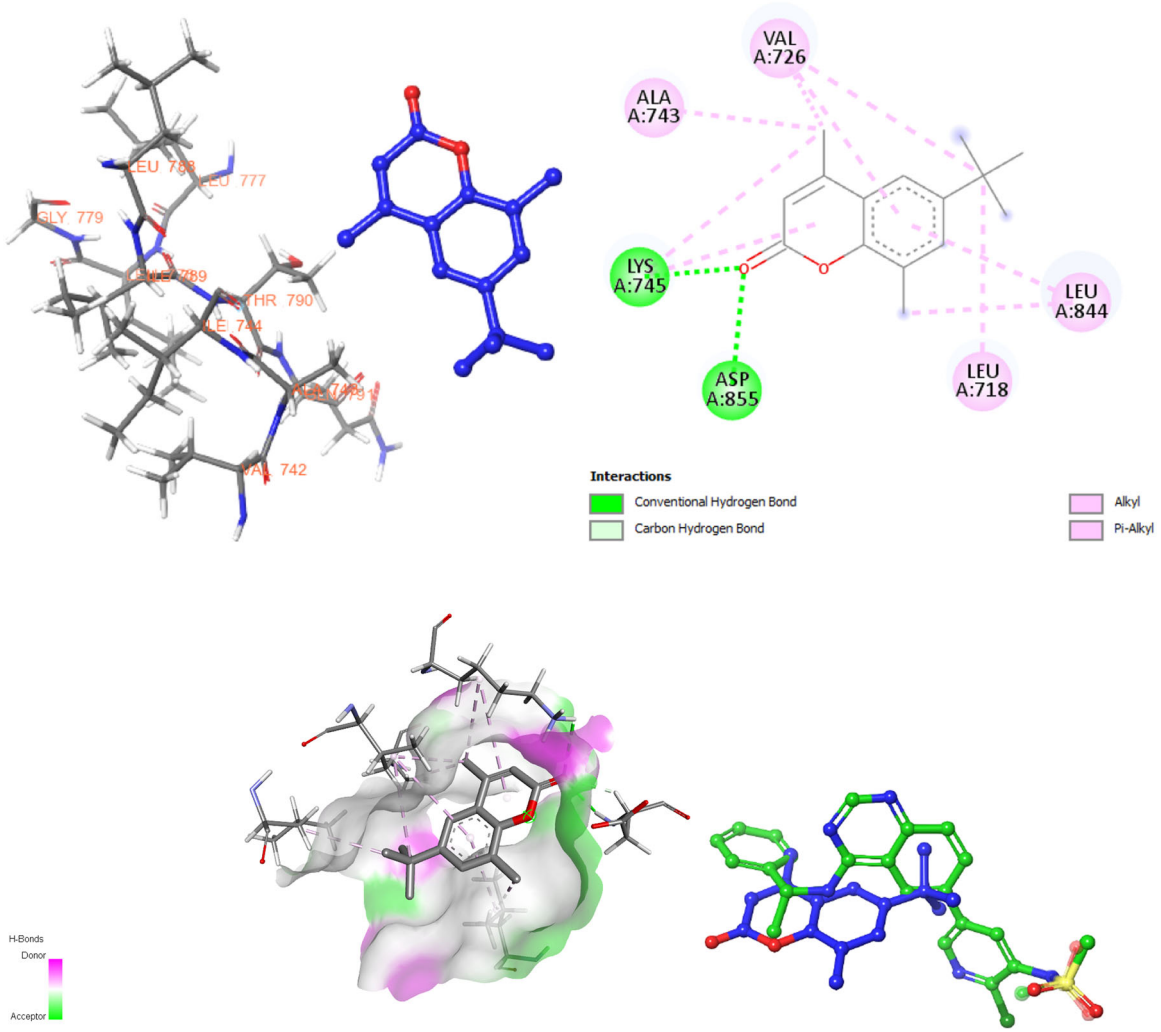

FIGURE 13 | The visualisation of the interactions of **3a** and EGFR, 3D, 2D, Hydrogen bonds and superimpose of **3a** and reference ligand 42Q.

pharmacophores highlights the mechanistic distinctiveness of this scaffold [22, 23, 47, 48].

In parallel with the obtained results, Velasco-Velazquez et al. reported that 4-hydroxycoumarin damages the actin cytoskeleton of murine melanoma cell lines without indicating any toxic effect on healthy fibroblast cell lines [49]. In another study, it has been stated that a coumarin derivative, which includes 1,2,4-triazolin-3-one attached to 4-methylcoumarin, has an anticancer effect in renal carcinoma cells [50]. Egan et al. have indicated that 8-nitro-7-hydroxycoumarin has cytotoxic activities and induces apoptosis in the human leukemia cells HL-60 and K562 [51]. Synthetic scopoletin derivatives exhibited powerful effects in human breast adenocarcinoma (MCF-7 and MDA-MB-231) and human colorectal adenocarcinoma (HT29) cells [52].

On the other hand, in silico inhibition effects on CDK9, VEGFR2, and EGFR of the used coumarin derivatives were determined to evaluate the potential mechanism of the synthesized compounds. When molecular docking results were evaluated, the **3a** molecule showed the best binding affinity with CDK9 at the level of $\Delta G = -8.1$ kcal/mol and interacted with one hydrogen bond with ASPA167 residue (Figure 7 and Table 2). Moreover, **3a** bounded with ALAA:166, VALA:79, LEUA:156, ALAA:46, ILEA:25 via alkyl bonds. In addition, it is bound with PHEA:103 by pi-pi-T-shaped. **3b** compound has not formed any hydrogen bonds but has created numerous alkyl bonds with different residues. The binding energy was calculated as -7.8 kcal/mol (Figure 8 and Table 2). It also created alkyl bonds with PHEA:105, ALAA:46, CYSA:106, VALA:79, ALAA:166, LEUA:156. In addition, pi-pi-T-shaped and pi-sigma bounds were seen between **3b** and the PHEA:103 residue. Lastly, the **3c** molecule created two hydrogen bonds with LYSA41 and ASPA145 residues, and the binding affinity was −8.1 kcal/mol (Figure 9 and Table 2). Furthermore, **3c** formed alkyl bonds with ALA A:39, VALA:26, and LEUA:134 residues. Reference ligand UT5 has a hydrogen bond with the CYS106 residue. The used compounds created hydrogen bonds with different residues. **3a** and **3c** exhibited equal binding affinity with CDK9 receptor. These results were found near the reference ligand score (Table 2). Hydrogen bonds stabilize the ligand–protein structures; in this way, these bonds play a critical role in molecular docking simulations. Especially, intermolecular hydrogen bonds have an important role in the prediction of binding accuracy [53]. Moreover, it has been reported that alkyl bonds are important for molecular docking studies and biological activity. Alkyl chains contribute to

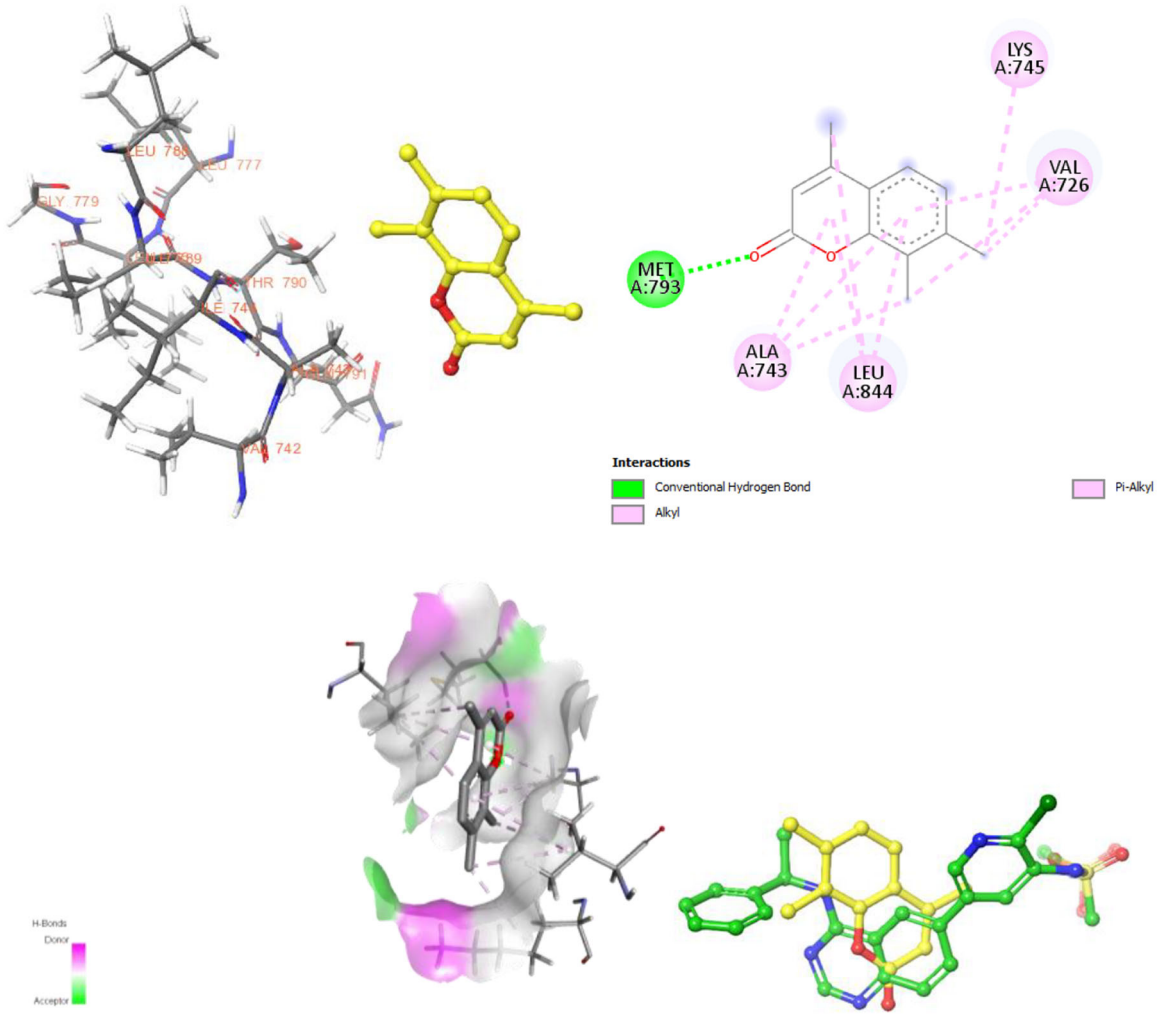

FIGURE 14 | The visualisation of the interactions of **3b** and EGFR, 3D, 2D, Hydrogen bonds and superimpose of **3b** and reference ligand D0D.

binding stability through hydrogen bonds, π-cation/anion and π-π interactions, as well as π-alkyl interactions, which help stabilize ligands in the active site [54]. The data showed that the compounds used showed strong interactions with target proteins.

When the molecular docking results of the VEGFR2 protein with the synthesized molecules were evaluated, **3a** compound showed the best binding affinity score as −8.9 kcal/mol (Figure 10 and Table 2). **3a** compound formed lots of alkyl bonds with LEUA:1035, PHEA:1047, ALAA:866, CYSA:919. In addition, **3a** formed pi-sigma bonds with LEUA:840 and VALA:848 residues. The binding energy of **3b** was calculated as −8.3 kcal/mol. The interaction of this compound did not form any hydrogen bonds but created many alkyl bonds with the VEGFR2 protein (Figure 11 and Table 2). **3b** created alkyl bonds with LEUA:840, ALAA:866, PHEA:918, CYSA:919, LEUA:1035, VALA:916, CYSA1045, VALA:899. It also created pi-sigma bonds with VALA:848 and PHEA:1047 residues. **3c** indicated a powerful interaction with the VEGFR2 receptor, and binding energy was −8.6 kcal/mol with several alkyl bonds (Figure 12 and Table 2). **3c** formed lots of alkyl bonds with PHEA:1047, VALA:848, ALAA:866, CYSA:919, LEUA:1035, VALA:899, VALA:916 and created pi-sigma bond with LEUA:840. But differently, the reference molecule 42Q formed hydrogen bonds with GLU:75, CYS:109, and ASP:236. The obtained affinity scores were lower than the reference ligand of the used protein structure (Table 2).

Next protein, EGFR, and synthesized compounds indicated good interactions. **3a** molecule binding affinity was found as −7.1 kcal/mol and 2 hydrogen bonds formed between LYSA745 and ASPA855 residues (Figure 13 and Table 2). **3a** created alkyl bonds with ALAA:743, VALA:726, LEUA:844 and LEUA:718. **3b** molecule showed a lower binding affinity according to the **3a** and **3c** compounds. The binding affinity of **3b** was −6.3 kcal/mol and formed only one hydrogen bond with META:793 (Figure 14 and Table 2). In addition, **3b** created alkyl bonds with ALAA:743, LEUA:844, LYSA:745 and VALA:726. Lastly, **the 3c molecule created two hydrogen bonds with GLYA:796 and CYSA:797 residues, and the** binding affinity was calculated as −6.8 kcal/mol (Figure 15 and Table 2). **3c** crerated alkyl bonds with META:793, LEUA:844, LEUA:792, ALAA:743, VALA:726, LYSA:745 residues. Differently, the reference molecule DOD formed a hydrogen bond with the MET:101 residue. The results of molecular docking studies indicated that the binding affinity scores of the synthesized molecules were lower than the reference ligand used in the protein structure. The superimposed models of all ligands with the proteins are shown in Figure 16, and the RMSD values are

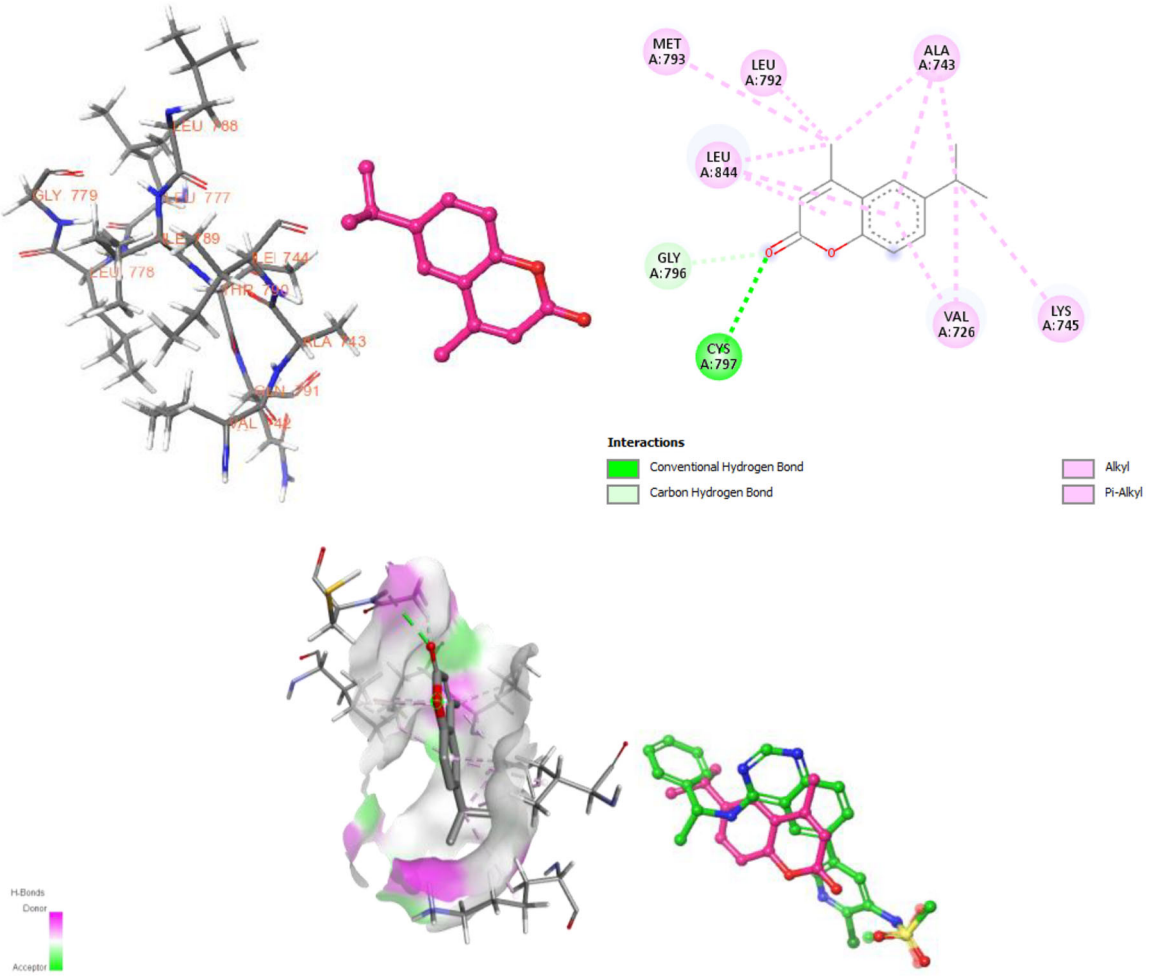

FIGURE 15 | The visualisation of the interactions of **3c** and EGFR, 3D, 2D, Hydrogen bonds and superimpose of **3c** and reference ligand D0D.

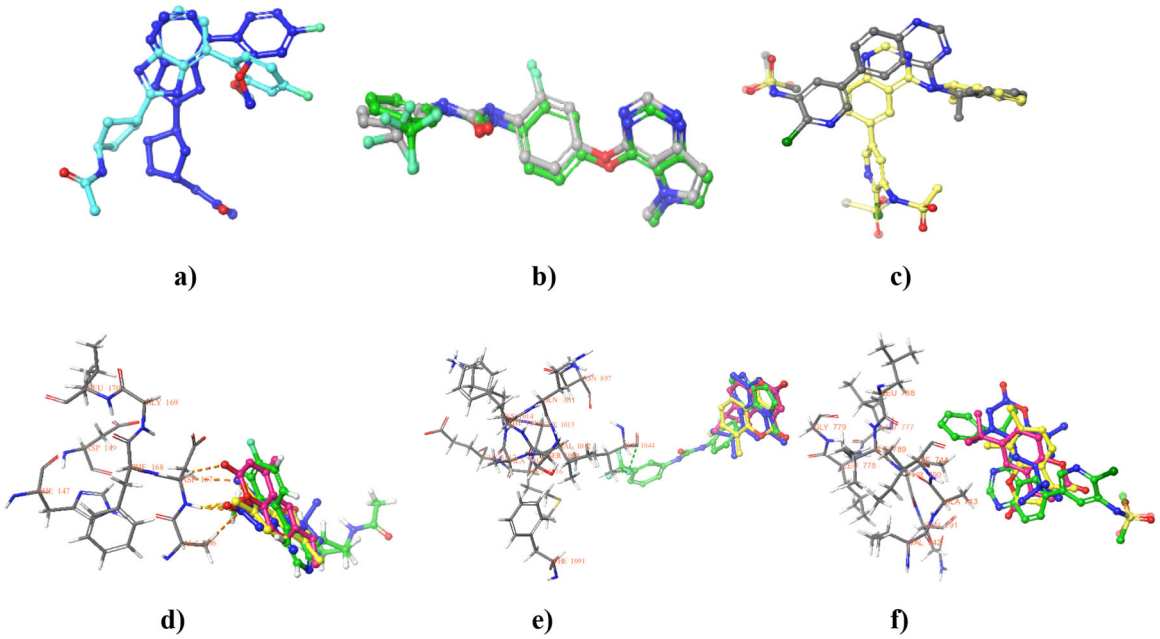

FIGURE 16 | Superimpose models of redocking (a) CDK9 (b) VEGFR2 (c) EGFR and all ligands with proteins (d) CDK9 (e) VEGFR2 (f) EGFR (**Reference ligands**: green, **3a**: blue, **3b**: yellow, **3c**:salomon pink).

reflected in Table 3. Molecular docking accuracy is typically determined by the root mean square deviation (RMSD) of the positions of all heavy atoms of the ligand in the docked position relative to those in the crystal structure. An RMSD value of the ligand of less than 2.0 Å is considered acceptable [55].

In a recent study, Kasmi et al. (2020) tested the anticancer effects of 24 coumarin derivatives on CDK protein in HepG-2 cells. At the end of the study, they declared that the best docking energy was −9.43 kcal/mol [56]. In another study, Abd El-Kerim et al. (2019) reported some thiazol-hydrazono-coumarin hybrids targeting CDK2 in human cervical cancer. In the study, they determined significant inhibitory effects of some hybrid molecules. In molecular docking studies, part of their study, they found several binding free energy levels between −13.00 kcal/mol and −13.66 kcal/mol when their reference molecule's binding free energy was −11.11 kcal/mol [57]. Shamsiya and Bahulayan (2022) synthesized some solid-state emitters based on oxazolone-coumarin-triazole with multi-component reaction as anti-breast cancer compounds. Moreover, they performed molecular docking studies on six synthesized compounds (**31 to 36**) with the CDK receptor. In the study, only 31.,32. and 36. molecules created hydrogen bonds with the receptor's LYS89 amino acid, and the docking score was −10 kcal/mol [58]. El Sayed et al (2022) tested 18 new structures of tri-azolecoumarin-glycosyl hybrid molecules and their tetrazole hybrid analogues as potent anticancer molecules. They determined **19.**, **20.** and **21.** molecules have good anticancer activity in PC-3, Paca-2, A-375, Mel-501, and Caco-2 cancer cell lines. As an important point, they declared that the coumarin groups formed hydrogen bonds with an important residue LEU83. In addition **20.** and **21.** molecules created hydrogen bonds with GLN131 and LYS129 respectively with free bonding energy between −10.76 kcal/mol and −10.85 kcal/

TABLE 3 | RMSD values of superimposed models.

Molecule	Target proteins		
	CDK9 RMSD	VEGFR2 RMSD	EGFR RMSD
3a	1.0115	0.7762	0.9532 Å
3b	1.0143	0.7901	1.2388 Å
3c	0.8120	0.5394	1.0648 Å
Re-docking RMSD Values			
UT5			1.0166 Å
D0D			1.3032 Å
42Q			0.5357 Å

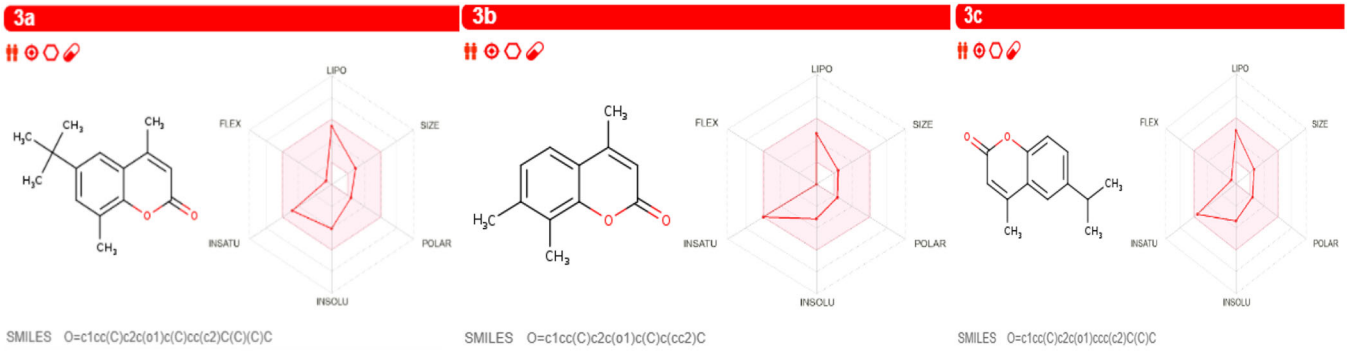

FIGURE 17 | Bioavailability radar scores of used compounds.

TABLE 4 | Prediction of physicochemical properties of the used compounds.

Molecule	MW	CHA	NAHA	FCsp3	NRB	NHBA	NHBD	MR	TPSA
3a	230.3 g/mol	17	10	0.40	1	2	0	71.69	30,21 A^2
3b	188.22 g/mol	14	10	0.25	0	2	0	57.38	30,21 A^2
3c	202.25 g/mol	15	10	0,31	1	2	0	62.03	30,21 A^2

Abbreviations: CHA, count of heavy atoms; FCsp3, fractionalised Csp3; MR, molar refractivity, MW, molecular mass; NAHA, number of aromatic heavy atoms; NHBA, number of hydrogen bond acceptors; NHBD, number of hydrogen bond donors; NRB, number of rotatable bonds; TPSA, topological polar area of the surface.

TABLE 5 | Prediction of lipophilicity features of the used compounds.

Molecule	Log Po/w (iLOGP)	Log Po/w (XLOGP3)	Log Po/w (WLOGP)	Log Po/w (MLOGP)	Log Po/w (SILICOS-IT)	Consensus Log Po/w
3a	3.02	3.86	3.71	3.32	4.63	3.71
3b	2.40	2.55	2.72	2.53	3.86	2.81
3c	2.65	2.95	3.22	2.80	3.91	3.11

mol. Moreover, the study outcomes indicated that compound 19 may be a good inhibitor for EGFR and VEGFR2 [59].

Beyaztaş et al (2024) synthesized a novel compound, 7-diethylamino-4-chloromethyl coumarin (referred to as 7D4C), and assayed against human epithelial adenocarcinoma (LoVo) and healthy fibroblast (CCD-18Co) cell lines. The targeting VEGFR2 (PDB ID: 1YWN) in silico molecular docking study data indicated -6.38 ± 0.43 kcal/mol binding score. This score was better than reference molecule [60]. Twenty azaheterocyclic coumarin derivatives were synthesized and their inhibition effect on VEGFR2 was investigated in a study by Ahmed et al (2021), which emphasized that 4a molecule showed an important inhibition activity on VEGFR2 (PDB ID:4ASD) and molecular docking score was determined as −7.0594 kcal/mol [61].

On the other hand, Gangadhar et al (2023) assessed the anticancer activities of some coumarin-piperazine 1,2,3-triazole hybrid compounds on MCF-7, MDA-MB-468, and MDA-MB-231 cancer cells. They stated that 7f and 7h have more important effects on EGFR than the standard drug erlotinib. Furthermore, they indicated that molecular docking studies on EGFR (PDB ID-4HJO) clearly showed 7e, 7f, 7h, and 7k have more powerful binding energies and Ki values than erlotinib. The binding free energies of synthesized compounds found as −9.58 kcal/mol, −10.67 kcal/mol, −10.50 kcal/mol, and −10.27 kcal/mol, respectively. Erlotinib′s bonding affinity was found as −7.69 kcal/mol. According to the study outcomes 7e formed 3 hydrogen bonds 7k and 7h created 2 hydrogen bonds with the receptor. When 7h did not have a hydrogen bond, erlotinib showed only one hydrogen bond [62]. In the study of Yadav et al. (2024), which synthesized new thiosemicarbazones (3a-d) of 3-acetylumbelliferone and Schiff's bases of 3-acetyl-coumarin as an anticancer agent against MCF-7 cells, in silico molecular docking results targeting EGFR, of the study showed that the used compounds have good binding scores than erlotinib. The best binding score was calculated as −10.1 kcal/mol [63]. Kecel-Gündüz et al (2023) tested the antioxidant and anticancer activity of a novel coumarin compound, 7-((8-(4-benzylpiperidin-1-yl)octyl)oxy)-4-methyl-2H-chromen-2-one. In the research, authors used EGFR (PDB ID: 1M17) as a target in a molecular docking study and the score was −5.24 kcal/mol [64]. In another research, which indicates anticancer effects of N (3)-alkyl incorporated-3-acetyl-4-hydroxycoumarin thiosemicarbazones and their copper(II) complexes by Shrestha et al (2024) reported that compounds 3,4 and 5 exhibited important free binding energies with EGFR receptor between −6.8 and −8.4 kcal/mol [65].

The ADME data indicated that all molecules used have good bioavailability radar scores (Figure 17). When synthesized compounds are evaluated according to Lipinski's 'rule of 5'; MW of all compounds are lower than 500. Furthermore, it has been reported that lipophilicity, which is measured by the Log P octanol-water solubility ratio, is associated with absorption. This is indicated by the distribution coefficient between octanol and water [25]. Log P values of all synthesized compounds are lower than 5 and all compounds has water-soluble features (ESOL model). When a drug candidate molecule is evaluated according to the Lipinski criteria, if there are violations of at least two rules, it is unlikely that the molecule is an oral drug, and the molecules used in this study fully comply with these criteria (Tables 4–7).

Veber et al. [66] evaluated the effect of polar properties and flexibility of the molecule on the oral bioavailability of a drug candidate molecule and reported that molecular stiffness plays an effective role in oral bioavailability. In addition, the permeability increases as the polar surface decreases. If the number of rotatable bonds increases, it affects the permeability rate negatively. It was reported that drug-candidate molecules with NRB $\leq$ 10 bonds and a polar surface area equal to or less than 140 Å^2 (TPSA $\leq$ 140 Å^2) are highly likely to be bioavailable in

TABLE 7 | Prediction of drug-likeness properties of the used compounds.

Parameters	3a	3b	3c
Lipinski	Yes	Yes	Yes
Ghose	Yes	Yes	Yes
Veber	Yes	Yes	Yes
Egan	Yes	Yes	Yes
Muegge	Yes	No; 1 violation MW < 200	Yes
Bioavailability score	0.55	0.55	0.55

TABLE 6 | Prediction of water solubility features of the used compounds.

Parameters	3a	3b	3c
Log S (ESOL)	−4.07	−3.14	−3.38
Solubility	1.96e-02mg/mL; 8.53e-05mol/L	1.36e-01mg/mL; 7.21e-04mol/L	8.44e-02mg/mL; 4.17e-04mol/L
Class	Moderately soluble	Soluble	Soluble
Log S (Ali)	−4.19	−2.83	−3.25
Solubility	1.48e-02mg/mL; 6.44e-05mol/L	2.77e-01mg/mL; 1.47e-03mol/L	1.15e-01mg/mL; 5.66e-04mol/L
Class	Moderately soluble	Soluble	Soluble
Log S (SILICOS-IT)	−5.60	−4.77	−4.83
Solubility	5.75e-04mg/mL; 2.49e-06 mol/L	3.17e-03mg/mL; 1.68e-0.5 mol/L	3.02e-03mg/mL; 1.49e-05mol/L
Class	Moderately soluble	Moderately soluble	Moderately soluble

rats. In the present study, the number of rotatable bonds of **3a,3b,3c** were detected as 1,0,1 respectively. Besides, TPSA value of title compounds was 30.21 $A^{2.}$. These data are in accordance with Veber's criteria (Tables 4, 5 and 7).

Ghose et al. [67] characterized the drugs used both quantitatively and qualitatively. In their studies, they made a quantitative analysis of their physicochemical properties, while their qualitative analysis took into account the functional groups. The ALog P value is expressed as WLog P in the SwissADME web tool [42]. When the compounds used in our research are evaluated according to Ghose's rules, it is seen that they are in full harmony (Tables 4, 5 and 7).

Muegge et al. [68] developed a simple filter that can distinguish between drug-like molecules and nondrug-like molecules. Their method is based on the criteria of poor functioning of nondrug compounds and elimination of those with less than two pharmacophore points and those with more than seven. The obtained results of our research show that **3a** and **3c** are in the range of these criteria. However, the **3b** molecule does not fully comply with these criteria, only because its molecular weight is less than 200 (Table 7).

The BOILED-Egg model (Brain or Gut Predictive Permeation Method) is a method for estimating passive gastrointestinal absorption of small parts and brain access, using mathematical expressions of Wlog P and TPSA values [69, 70]. The TPSA is a molecular identifier for orally active drugs that correlates well with passive transport, and its value should be less than approximately 120 $Å^2$ [71, 72]. Additionally, it has been reported that orally administered molecules with a small polar surface area (less than 60–70 $Å^2$) can cross the blood-brain barrier and enter the central nervous system (CNS), making them potential agents for treating CNS diseases [73]. The BOILED-Egg model of the used compounds is shown in Figure 13. The yellow area represents compounds predicted to penetrate the blood-brain barrier, while the white area represents the physicochemical domain showing compounds predicted to indicate human intestinal absorption. These regions are interrelated. Since all of these molecules are in the yellow area, they are not removed from the central nervous system via P-glycoprotein [25]. This reveals that the compounds used in the study can be potential drug candidates for the treatment of brain cancer and/or central nervous system diseases (Figure 18).

In humans, the cytochrome P450 family consists of 57 isozymes that have a function in normal metabolic activities, affect the pharmacokinetics of drugs, and cause adverse effects in patients with drug-drug interactions [74, 75]. Therefore, examining the interactions of CYPs with drug candidate molecules is important in drug design [25]. In the presented study, the interactions of the title compounds with CYP isoenzymes were estimated using the in silico SwissADME tool. The used molecules are expected to inhibit only one enzyme. The compounds used in the study may inhibit CYP1A2, which mediates the metabolic rate, which may result in increased toxic effects (Table 8). Since CYP1A2 metabolizes some drugs, including theophylline, propranolol, and clozapine, inhibition of this enzyme may cause unfavorable drug-drug interactions [76]. This prediction score needs to be corrected via further studies.

PAINS (Pan-Assay Interference Compounds) are chemical structures that may cause false positives during high-throughput scanning. Rather than affecting a specifically identified target, these compounds interact nonspecifically with many biological targets [77, 78]. SwissADME gives a warning when there are such parts in the molecule. As seen from Table 9, there is no violation. These prediction data show that

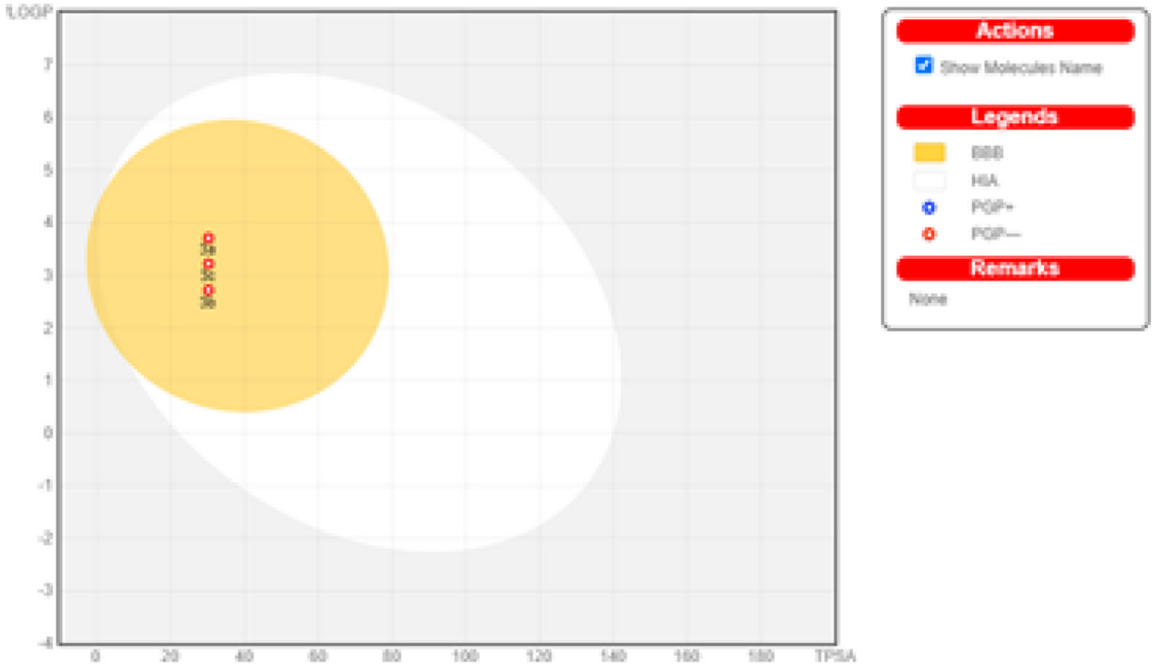

FIGURE 18 | BOILED-Egg determination of the used compounds. The BOILED egg predicts the passive permeability of the BBB, gastrointestinal reabsorption, and the presence of P-gp.

TABLE 8 | Predicted pharmacokinetic determination of the used compounds.

Parameters	3a	3b	3c
GI absorption	High	High	High
BBB permeant	Yes	Yes	Yes
P-gp substrate	No	No	No
CYP1A2 inhibitor	Yes	Yes	Yes
CYP2C19 inhibitor	No	No	No
CYP2C9 inhibitor	No	No	No
CYP2D6 inhibitor	No	No	No
CYP3A4 inhibitor	No	No	No
Log Kp (skin permeation)	−4.96 cm/s	−5.64 cm/s	−5.44 cm/s

Abbreviations: BBBper, blood-brain penetration; CYP, cytochromes; GI abs, gastrointestinal uptake; P-gp sub, P-glycoprotein as a substrate.

TABLE 9 | Predicted medicinal chemistry determination of the used compounds.

Parameters	3a	3b	3c
PAINS	0 alert	0 alert	0 alert
Brenk	1 alert: Coumarin	1 alert: Coumarin	1 alert: Coumarin
Leadlikeness	No:2 violations: MW < 250, XLOGP3 > 3.5	No;1 violation MW < 250	No;1 violation MW < 250
Synthetic accessibility	3.02	2.92	2.74

Note: SwissADME predictions showed that our compounds comply with Lipinski's five rules and the Ghose, Egan, and Veber rules. LogP values ranged from 2.8 to 3.71, indicating moderate lipophilic properties, and topological polar surface area (TPSA) values were calculated to be < 75 Å². These parameters are consistent with high oral bioavailability potential and the possibility of crossing the blood-brain barrier (BBB) via passive diffusion. Furthermore, BOILED-Egg model results indicated that the compounds presented a suitable profile in terms of both gastrointestinal absorption and potential BBB permeability (Table 8). A negative prediction was obtained regarding P-gp substrate potential, supporting the drug candidate potential for central nervous system tumors.

TABLE 10 | In silico toxic activity prediction of the used compounds via Protox II.

	Oral Toxicity		Organ toxicity, toxicity prediction/probability and endpoints				
				Toxicity endpoints			
Molecule	LD50 (mg/kg)	Toxicity Class	Organ toxicity Hepatotoxicity	Carcinogenicity	Immunotoxicity	Mutagenicity	Cytotoxicity
3a	3800	V	Inactive 0.77	Active 0.54	Inactive 0.97	Inactive 0.71	Inactive 0.66
3b	3800	V	Inactive 0.70	Active 0.55	Inactive 0.96	Inactive 0.65	Inactive 0.65
3c	3800	V	Inactive 0.73	Active 0.53	Inactive 0.98	Inactive 0.70	Inactive 0.58

the compounds used in the study cannot cause false-positive results and are suitable for further biological activity tests.

The SwissADME web tool identifies a structural violation in the medicinal chemistry section, comprising a list of 105 compounds that are presumably toxic, chemically reactive, metabolically unstable, or exhibit weak pharmacokinetic properties [79]. Brenk et al. [79] defined undesirable structures and evaluation criteria to enrich lead-like structures that facilitate the interaction between direct structure and activity. In the medical chemistry section, SwissADME gives a structural warning from the coumarin ring for all used compounds. Because the coumarin ring has double bonds, which SwissADME shows as a violation. The structure's double bond can be oxidized by cytochrome P-450 and covalently bound to proteins [68, 69]. The compounds used in the study did not pass the Brenk filter, presumably due to potential receptor binding and instability (Table 9). In addition, Teague et al. [42] suggested that molecules with MWT = 100-350 and ClgP = 1-3.0 are superior to other drug-like compounds. According to these results, **3b** and **3c** compounds agree with the criteria of Teague et al. [80] (Table 7).

Daina et al. [42] set up a piece-meal method system in their study, in which they analyzed more than 13 million compounds, and scored if the more common molecular fragments have higher synthetic accessibility (SA), while rare structures show SA after a difficult synthesis. In this rating, they ranked accessibility from 1 (very easy) to 10 (very difficult). In our study, the obtained results reflect SA scores of title compounds

that range from 2.74 to 3.02, which means that the synthesis of these compounds is easy (Table 9). Furthermore, toxicity analysis is an important step in the discovery of new drugs. Predicting the toxicity properties of a drug candidate molecule can minimize payments, time, and the need for in vitro testing. Various virtual tools based on known databases can be used to test at an early stage and eventually determine the drug feasibility of the substance. In the presented study, the Protox-II web tool was used to estimate the potential toxic properties of the compounds used in the research [81–83]. The predicted data show that all molecules have an LD50 of 3800 mg/kg and belong to toxicity class V ($2000 < LD50 \leq 5000$). This is an indication that the synthesised molecules may be harmful by ingestion. In addition, with a probability score ranging from 0.7 to 0.77, the prediction of organ toxicity indicates that the compounds do not possess hepatotoxic properties. In addition, it was observed that the tested compounds fall into the group of potential carcinogens with a low probability of 0.53–0.55. The data obtained indicate a low to moderate carcinogenic effect. Although these scores are noteworthy, further studies are needed to compare these prediction results with in vitro and in vivo studies. Moreover, all compounds were predicted as non-immunotoxins, non-mutagenic, and non-cytotoxic. Finally, the nuclear binding prediction/probability score of synthesized molecules was predicted for seven different toxicity targets (Tables 10 and 11). According to the Protox-II tool predictions, the tested molecules did not show any interactions with the selected targets.

In conclusion, the presented data from in vitro studies indicate that all the coumarin derivatives used exhibit a very high cytotoxic action potential on human neuroblastoma cell lines. While **3a** and **3c** showed vigorous selective activity against human neuroblastomas, **3b** showed selective activity depending on concentration. Molecular docking scores were also in line with the in vitro studies. The obtained results of molecular docking studies indicated that **3a** molecule has the best affinity score on all proteins. Its binding affinities were $\Delta G = -8.1$ kcal/mol, $\Delta G = -8.9$ kcal/mol, $\Delta$and $G = 7.1$ kcal/mol for CDK9, VEGFR2, and EGFR, respectively. When **3b** showed the best binding affinity on VEGFR2 ($\Delta G = -8.3$ kcal/mol), 3c indicated the best binding score on CDK9 ($\Delta G = -8.1$ kcal/mol). These data clearly showed that *in silico* and in vitro studies are in agreement with each other. When the compounds used were evaluated according to their *in silico* physicochemical features, they demonstrated full agreement, while only the **3b** molecule showed a small deviation in drug-likeness activity. In the evaluation of medical chemistry prediction, the title molecules have no violation of PAINS, while according to Brenk, all molecules indicated one alert. In addition, when **3a** and **3c** are in agreement with drug-likeness features of Lipinski, Ghose, Veber, Egan, and Muegge criteria, **3b** was in disagreement with only the Muegge criteria. The molecules used showed a selective inhibition effect on the CYP1A2 enzyme, which shows that the molecules may induce undesirable drug-drug interactions. BOILED-Egg analysis results indicate that these molecules can be beneficial in the treatment of brain cancer and CNS diseases. Furthermore, Protox II prediction demonstrated that the title compounds have a slight carcinogenic effect but did not exhibit predicted hepatotoxicity, cytotoxicity, immunogenic toxicity, and mutagenicity, and they are in class V of oral toxicity.

TABLE 11 | The nuclear interaction scores of the compounds used via Protox II.

Molecule	Aryl hydrocarbon receptor (AhR)	Androgen receptor (AR)	Androgen receptor ligand binding domain (AR-LBD)	Aromatase	Estrogen receptor alpha (ER)	Estrogen receptor ligand binding domain (ER-LBD)	Peroxisome proliferator activated receptor gamma (PPAR-Gamma)
3a	Inactive	Inactive	Inactive	Inactive	Inative	Inactive	Inactive
	0.76	0.98	0.98	0.98	0.86	0.93	0.98
3b	Inactive	Inactive	Inactive	Inactive	Inactive	Inactive	Inactive
	0.62	0.93	0.94	0.90	0.76	0.97	0.9
3c	Inactive	Inactive	Inactive	Inactive	Inactive	Inactive	Inactive
	0.70	0.97	0.99	0.93	0.73	0.98	0.98

Note: ProTox-II predictions determined the oral LD_{50} values of our compounds to be 3800 mg/kg and classified their toxicity level as V ($2000 < LD_{50} \leq 5000$). The predicted probabilities for carcinogenicity were in the range of 53%–55% (Table 10). ProTox-II yielded negative results for mutagenicity and immunotoxicity for all compounds. These parameters were evaluated as merely hypothesis-generating, considering the limitations of the in silico model.

Moreover, in silico nuclear binding predictions were negative for the used molecules. Although in silico studies show that the biocompatibility, BBB crossing, and drug-like properties of the molecules used are at the desired level, these results need to be confirmed by both in vitro and in vivo experiments.

As a result, it was observed that the tested molecules, especially **3a** and **3c**, have promising effects by acting as direct, selective, and cytotoxic compounds. Molecular docking study data were in parallel with in vitro studies. Further, it is estimated that coumarin compounds evaluated via SwissADME and Protox-II web tools have preferred physicochemical and ADMET properties and showed very slight toxic activity. These results indicated that the synthesized molecules have multi-target properties and all molecules are suitable drug candidates for further preclinical studies.

Author Contributions

Conceptualization: Hasan Turkez, Fatih Caglar Celikezen, and Mehmet Enes Aslan. Methodology: Kamuran Sarac, Fatih Caglar Celikezen, Mehmet Enes Aslan, Sena Oner. Software: Fatih Caglar Celikezen. Writing – original draft preparation: Hasan Turkez, Fatih Caglar Celikezen, Kamuran Sarac, Ercan Seyhan, and Mehmet Enes Aslan. Writing – review and editing: Hasan Turkez, Fatih Caglar Celikezen, Ercan Seyhan and Mehmet Enes Aslan. All authors have read and agreed to the published version of the manuscript.

Conflicts of Interest

H.T. is the founder and shareholder of Bash Biotech Inc., San Diego, CA, USA. The other authors declare no competing interests.

Data Availability Statement

The datasets used and/or analyzed during the current study are available from the corresponding author upon reasonable request.

References

1. World Health Organization, "Cancer," published 2018, https://www.who.int/news-room/fact-sheets/detail/cancer.

2. J. M. Maris, M. D. Hogarty, R. Bagatell, and S. L. Cohn, "Neuroblastoma," *Lancet* 369, no. 9579 (2007): 2106–2120.

3. G. Schleiermacher, H. Rubie, O. Hartmann, et al., "Treatment of Stage 4s Neuroblastoma—Report of 10 Years' Experience of the French Society of Paediatric Oncology (SFOP)," *British Journal of Cancer* 89 (2003): 470–476.

4. V. P. Tolbert and K. K. Matthay, "Neuroblastoma: Clinical and Biological Approach to Risk Stratification and Treatment," *Cell and Tissue Research* 372 (2018): 195–209.

5. A. M. Waters, J. E. Stewart, V. R. Atigadda, et al., "Preclinical Evaluation of a Novel rxr Agonist for the Treatment of Neuroblastoma," *Molecular Cancer Therapeutics* 14, no. 7 (2015): 1559–1569.

6. M. Monje and J. Dietrich, "Cognitive Side Effects of Cancer Therapy Demonstrate a Functional Role for Adult Neurogenesis," *Behavioural Brain Research* 227 (2012): 376–379.

7. Y. Bai, D. Li, T. Zhou, et al., "Coumarins From the Roots of Angelica Dahurica With Antioxidant and Antiproliferative Activities," *Journal of Functional Foods* 20 (2016): 453–462.

8. M. Jadhav, R. S. Kalhapure, S. Rambharose, C. Mocktar, and T. Govender, "Synthesis, Characterization and Antibacterial Activity of Novel Heterocyclicquaternary Ammonium Surfactants," *Journal of Industrial and Engineering Chemistry* 47 (2017): 405–414.

9. H. A. H. Elshemy and M. A. Zaki, "Design and Synthesis of New Coumarin Hybrids and Insight Into Their Mode of Antiproliferative Action," *Bioorganic & Medicinal Chemistry* 25, no. 3 (2017): 1066–1075.

10. M. Martinez-Amezaga, R. A. Giordano, D. N. Prada Gori, et al., "Synthesis of Propargylamines via the a (3) Multicomponent Reaction and Their Biological Evaluation as Potential Anticancer Agents," *Organic & Biomolecular Chemistry* 18 (2020): 2475–2486.

11. A. Thirupathi, C. M. Shanmugavadivelu, and S. Natarajan, "Fastidious Anatomization of Biota Procured Compounds on Cancer Drug Discovery," *Current Pharmaceutical Biotechnology* 21, no. 5 (2020): 354–363, https://doi.org/10.2174/1389201020666191128145015.

12. K. R. Campos, P. J. Coleman, J. C. Alvarez, et al., "The Importance of Synthetic Chemistry in the Pharmaceutical Industry," *Science* 363, no. 6424 (January 2019): eaat0805, https://doi.org/10.1126/science.aat0805.

13. D. A. Chan and A. J. Giaccia, "Harnessing Synthetic Lethal Interactions in Anticancer Drug Discovery," *Nature Reviews Drug Discovery* 10 (2011): 351–364, https://doi.org/10.1038/nrd3374.

14. J. Klenkar and M. Molnar, "Natural and Synthetic Coumarins as Potential Anticancer Agents," *Journal of Chemical and Pharmaceutical Research* 7 (2015): 1223–1238.

15. U. Rashid, F. Rahim, M. Taha, et al., "Synthesis of 2-acylated and Sulfonated 4-hydroxycoumarins: In Vitro Urease Inhibition and Molecular Docking Studies," *Bioorganic Chemistry* 66 (2016): 111–116.

16. D. Cao, Y. Liu, W. Yan, et al., "Design, Synthesis, and Evaluation of In Vitro and In Vivo Anticancer Activity of 4-substituted Coumarins: A Novel Class of Potent Tubulin Polymerization Inhibitors," *Journal of Medicinal Chemistry* 59, no. 12 (2016): 5721–5739.

17. M. Kaur, S. Kohli, S. Sandhu, Y. Bansal, and G. Bansal, "Coumarin: A Promising Scaffold for Anticancer Agents," *Anti–Cancer Agents in Medicinal Chemistry* 15 (2015): 1032–1048.

18. S. Emami and S. Dadashpour, "Current Developments of Coumarin-Based Anti–Cancer Agents in Medicinal Chemistry," *European Journal of Medicinal Chemistry* 102 (2015): 611–630.

19. E. H. Maleki, A. R. Bahrami, H. Sadeghian, and M. M. Matin, "Discovering the Structure–Activity Relationships of Different O-Prenylated Coumarin Derivatives as Effective Anticancer Agents in Human Cervical Cancer Cells," *Toxicology In Vitro* 63 (2020): 104745.

20. O. S. Ipek, B. O. Sucu, S. Gul, C. Yolacan, and M. Guzel, "Synthesis of Novel Hybrid Lonidamine–Coumarin Derivatives and Their Anticancer Activities," *Journal of Molecular Structure* 1281 (2023): 135114.

21. M. Holiyachi, S. L. Shastri, B. M. Chougala, et al., "Design and Synthesis of New Series of Dipyrromethane–Coumarin and Porphyrin–Coumarin Derivatives: Excellent Anticancer Agents," *Journal of Molecular Structure* 1237 (2021): 130424.

22. T. Al-Warhi, A. Sabt, E. B. Elkaeed, and W. M. Eldehna, "Recent Advancements of Coumarin-Based Anticancer Agents: An Up-To-Date Review," *Bioorganic Chemistry* 103 (2020): 104163.

23. A. K. Yadav, R. Maharjan Shrestha, and P. N. Yadav, "Anticancer Mechanism of Coumarin-Based Derivatives," *European Journal of Medicinal Chemistry* 267 (2024): 116179.

24. Y. Wang, J. Xing, Y. Xu, et al., "In Silico ADME/T Modelling for Rational Drug Design," *Quarterly Reviews of Biophysics* 48 (2015): 488–515.

25. T. L. Šestić, J. J. Ajduković, M. A. Marinović, E. T. Petri, and M. P. Savić, "In Silico ADMET Analysis of the a-, b- and d-Modified Androstane Derivatives With Potential Anticancer Effects," *Steroids* 189 (2023): 109147.

26. K. K. Sarkar, T. Mitra, M. A. Rahman, et al., "In Vivo Bioactivities of Hoya Parasitica (Wall.) and In Silico Study Against Cyclooxygenase Enzymes," *BioMed Research International* 1 (2022): 1–20.

27. L. Jia, S. Gao, Y. Y. Zhang, L. X. Zhao, Y. Fu, and F. Ye, "Fragmenlt Recombination Design, Synthesis, and Safener Activity of Novel Ester-Substituted Pyrazole Derivatives," *Journal of Agricultural and Food Chemistry* 69 (2021): 8366–8379.

28. E. Yilmaz and A. Cukurovali, "Synthesis, Characterization, Investigation of Biological Activity, Docking Studies, and Spectroscopic Properties of Hydrazone Compounds Containing Different Substituents," *Canadian Journal of Physics* 97, no. 4 (2019): 408–416.

29. M. A. Hossain, "Targeting the RAS Upstream and Downstream Signaling Pathway for Cancer Treatment," *European Journal of Pharmacology* 979 (September 2024): 176727, https://doi.org/10.1016/j.ejphar.2024.176727.

30. Y. Li, Q. Guo, C. Zhang, et al., "Discovery of a Highly Potent, Selective and Novel CDK9 Inhibitor as an Anticancer Drug Candidate," *Bioorganic & Medicinal Chemistry Letters* 27, no. 15 (2017): 3231–3237.

31. P. Maiti, M. Nand, T. Joshi, M. A. Ramakrishnan, and S. Chandra, "Identification of Luteolin -7-glucoside and Epicatechin Gallate From *Vernoniacinerea*, as Novel EGFR L858R Kinase Inhibitors Against Lung Cancer: Docking and Simulation-Based Study," *Journal of Biomolecular Structure and Dynamics* 39, no. 14 (September 2021): 5048–5057, https://doi.org/10.1080/07391102.2020.1784791.

32. H. M. Roaiah, I. A. Y. Ghannam, I. H. Ali, et al., "Design, Synthesis, and Molecular Docking of Novel Indole Scaffold-Based VEGFR-2 Inhibitors as Targeted Anticancer Agents," *Archiv der Pharmazie* 351, no. 2 (February 2018): e1700299, https://doi.org/10.1002/ardp.201700299.

33. F. Sangande, E. Julianti, and D. H. Tjahjono, "Ligand-Based Pharmacophore Modeling, Molecular Docking, and Molecular Dynamic Studies of Dual Tyrosine Kinase Inhibitor of EGFR and VEGFR2," *International Journal of Molecular Sciences* 21 (2020): 7779, https://doi.org/10.3390/ijms21207779.

34. H. Watanabe, E. Ichihara, H. Kayatani, et al., "VEGFR2 Blockade Augments the Effects of Tyrosine Kinase Inhibitors by Inhibiting Angiogenesis and Oncogenic Signaling in Oncogene-Driven Non-Small–Cell Lung Cancers," *Cancer Science* 112, no. 5 (May 2021): 1853–1864, https://doi.org/10.1111/cas.14801; Erratum in: *Cancer Sci* 113, no. 1 (January 2022): 365, https://doi.org/10.1111/cas.15219.

35. R. Mandal, S. Becker, and K. Strebhardt, "Targeting CDK9 for Anti–Cancer Therapeutics," *Cancers* 13 (2021): 2181, https://doi.org/10.3390/cancers13092181.

36. P. Wee and Z. Wang, "Epidermal Growth Factor Receptor Cell Proliferation Signaling Pathways," *Cancers* 9, no. 5 (May 2017): 52, https://doi.org/10.3390/cancers9050052.

37. S. Tamura, H. Hosoi, Y. Kuwahara, et al., "Induction of Apoptosis by an Inhibitor of EGFR in Neuroblastoma Cells," *Biochemical and Biophysical Research Communications* 358, no. 1 (June 2007): 226–232, https://doi.org/10.1016/j.bbrc.2007.04.124.

38. C. Zheng, R. Shen, K. Li, et al., "Epidermal Growth Factor Receptor Is Overexpressed in Neuroblastoma Tissues and Cells," *Acta biochimica et biophysica Sinica* 48, no. 8 (June 2016): 762–767, https://doi.org/10.1093/abbs/gmw064.

39. G. A. Smith, G. W. Fearnley, D. C. Tomlinson, M. A. Harrison, and S. Ponnambalam, "The Cellular Response to Vascular Endothelial Growth Factors Requires Co–Ordinated Signal Transduction, Trafficking and Proteolysis," *Bioscience Reports* 35, no. 5 (August 2015): e00253, https://doi.org/10.1042/BSR20150171.

40. E. A. Beierle, W. Dai, M. R. Langham, Jr., E. M. Copeland, 3rd, and M. K. Chen, "VEGF Receptors Are Differentially Expressed by Neuroblastoma Cells in Culture," *Journal of Pediatric Surgery* 38, no. 3 (March 2003): 514–521, https://doi.org/10.1053/jpsu.2003.50091.

41. S. Patamawadee, P. Dumnoensun, C. Arthit, S. Kanoknetr, and S. Rungnapha, "Synthesis of Propargylamine Mycophenolate Analogues and Their Selective Cytotoxic Activity Towards Neuroblastoma SH-SY5Y Cell Line," *Bioorganic & Medicinal Chemistry Letters* 45 (2021): 128135.

42. A. Daina, O. Michielin, and V. Zoete, "SwissADME: A Free Web Tool to Evaluate Pharmacokinetics, Drug-Likeness and Medicinal Chemistry Friendliness of Small Molecules," *Scientific Reports* 7 (2017): 42717.

43. V. Ngoc Toan, N. Dinh Thanh, and N. Minh Tri, "1,3,4-Thiadiazoline Coumarin Hybrid Compounds Containing d-Glucose/d-Galactose Moieties: Synthesis and Evaluation of Their Antiproliferative Activity," *Arabian Journal of Chemistry* 14 (2021): 103053.

44. H. Singh, J. V. Singh, K. Bhagat, et al., "Rational Approaches, Design Strategies, Structure Activity Relationship and Mechanistic Insights for Therapeutic Coumarin Hybrids," *Bioorganic & Medicinal Chemistry* 27 (2019): 3477–3510.

45. R. B. Myers, M. Parker, and W. E. Grizzle, "The Effects of Coumarin and Suramin on the Growth of Malignant Renal and Prostatic Cell Lines," *Journal of Cancer Research and Clinical Oncology* 120 (1994): S11–S13.

46. J. Bronikowska, E. Szliszka, D. Jaworska, Z. P. Czuba, and W. Krol, "The Coumarin Psoralidin Enhances Anticancer Effect of Tumor Necrosis Factor-Related Apoptosis-Inducing Ligand (TRAIL)," *Molecules* 17 (2012): 6449–6464.

47. S. H. Emam, R. A. Hassan, E. O. Osman, et al., "Coumarin Derivatives With Potential Anticancer and Antibacterial Activity: Design, Synthesis, VEGFR-2 and DNA Gyrase Inhibition, and In Silico Studies," *Drug Development Research* 84, no. 3 (2023): 475–499.

48. E. Y. Ahmed, O. M. Abdelhafez, D. Zaafar, et al., "Antitumor and Multikinase Inhibition Activities of Some Synthesized Coumarin and Benzofuran Derivatives," *Archiv der Pharmazie* 355 (2022): e2100327, https://doi.org/10.1002/ardp.202100327.

49. M. Velasco-Velazquez, "4-Hydroxycoumarin Disorganizes the Actin Cytoskeleton in B16-F10 Melanoma Cells but Not in B82 Fibroblasts, Decreasing Their Adhesion to Extracellular Matrix Proteins and Motility," *Cancer Letters* 198 (2003): 179–186.

50. P. P. Kattimani, R. R. Kamble, M. Y. Kariduraganavar, A. Dorababu, and R. K. Hunnur, "Synthesis, Characterization and In Vitro Anticancer Evaluation of Novel 1,2,4-triazolin-3-one Derivatives," *European Journal of Medicinal Chemistry* 62 (April 2013): 232–240, https://doi.org/10.1016/j.ejmech.2013.01.004.

51. D. Egan, P. James, D. Cooke, and R. O'Kennedy, "Studies on the Cytostatic and Cytotoxic Effects and Mode of Action of 8-Nitro-7-Hydroxycoumarin," *Cancer Letters* 118 (1997): 201–211.

52. W. Liu, J. Hua, J. Zhou, et al., "Synthesis and In Vitro Antitumor Activity of Novel Scopoletin Derivatives," *Bioorganic & Medicinal Chemistry Letters* 22, no. 15 (August 2012): 5008–5012, https://doi.org/10.1016/j.bmcl.2012.06.014.

53. M. J. R. Yunta, "It Is Important to Compute Intramolecular Hydrogen Bonding in Drug Design?," *American Journal of Modeling and Optimization* 5, no. 1 (2017): 24–57.

54. A. Balkrishna, S. Pokhrel, and A. Varshney, "Comparative COX I Molecular Docking of Phyto–Chemicals (Flavonoids, Alkaloids, Lignans and Terpenoids) for Anti-Platelet Aggregation Dynamics," *Current Computer-Aided Drug Design* 17, no. 4 (2021): 571–578, https://doi.org/10.2174/1573409916666200630110711.

55. W. Xiao, D. Wang, Z. Shen, S. Li, and H. Li, "Multi-Body Interactions in Molecular Docking Program Devised With Key Water Molecules in Protein Binding Sites," *Molecules* 23, no. 9 (September 2018): 2321.

56. R. Kasmi, E. Hadaji, O. Chedadi, A. El Aissouq, M. Bouachrine, and A. Ouammou, "2D-QSAR and Docking Study of a Series of Coumarin Derivatives as Inhibitors of CDK (Anticancer Activity) With an Application of the Molecular Docking Method," *Heliyon* 6, no. 8 (August 2020): e04514, 2020.e04514, https://doi.org/10.1016/j.heliyon.

57. S. S. Abd El-Karim, Y. M. Syam, A. M. El Kerdawy, and T. M. Abdelghany, "New Thiazol-Hydrazono─Coumarin Hybrids Targeting Human Cervical Cancer Cells: Synthesis, CDK2 Inhibition, QSAR and Molecular Docking Studies," *Bioorganic Chemistry* 86 (2019): 80–96, https://doi.org/10.1016/j.bioorg.2019.01.026.

58. A. Shamsiya and D. Bahulayan, "D–A Systems Based on Oxazolone–Coumarin Triazoles as Solid-State Emitters and Inhibitors of Human Cervical Cancer Cells (HeLa)," *New Journal of Chemistry* 46, no. 2 (2022): 480–489.

59. W. A. El-Sayed, F. M. Alminderej, M. M. Mounier, E. S. Nossier, S. M. Saleh, and A. F. Kassem, "Novel 1,2,3-Triazole─Coumarin Hybrid Glycosides and Their Tetrazolyl Analogues: Design, Anticancer Evaluation and Molecular Docking Targeting EGFR, VEGFR-2 and CDK-2," *Molecules* 27, no. 7 (March 2022): 2047, https://doi.org/10.3390/molecules27072047.

60. H. Beyaztas, K. Bozali, S. Koc, M. Ozdemir, B. Yalcin, and E. M. Guler, "Synthesis and Characterization of 7-diethylamino-4─Chloromethyl Coumarin: Spectroscopic Analysis, Molecular Docking, and Anticancer Activity on Large Intestine Carcinoma Cells," *Chemico-Biological Interactions* 404 (2024): 111287.

61. E. Y. Ahmed, W. S. Elserwy, M. F. El-Mansy, et al., "Angiokinase Inhibition of VEGFR-2, PDGFR and FGFR and Cell Growth Inhibition in Lung Cancer: Design, Synthesis, Biological Evaluation and Molecular Docking of Novel Azaheterocyclic Coumarin Derivatives," *Bioorganic & Medicinal Chemistry Letters* 48 (September 2021): 128258, https://doi.org/10.1016/j.bmcl.2021.128258.

62. K. H. Gangadhar, V. Benarjee, and A. Ratnamala, "Coumarin-Piperazine Tethered 1,2,3-Triazoles: EGFR Targeting Anti-Breast Cancer Evaluation and Molecular Docking Studies," *Polycyclic Aromatic Compounds* 44, no. 8 (2023): 5487–5503, https://doi.org/10.1080/10406638.2023.2265026.

63. A. K. Yadav, N. Singh, M. Silwal, A. Adhikari, and P. N. Yadav, "Synthesis, Characterization, Anticancer Activity, Molecular Docking and DFT Calculation of 3-acetylcoumarin Thiosemicarbazones and Schiff's Bases," *Results in Chemistry* 11 (2024): 101794.

64. S. Kecel-Gunduz, Y. Budama-Kilinc, B. Bicak, et al., "New Coumarin Derivative With Potential Antioxidant Activity: Synthesis, DNA Binding and In Silico Studies (Docking, MD, ADMET)," *Arabian Journal of Chemistry* 16, no. Issue 2 (2023): 104440.

65. R. M. Shrestha, K. Mahiya, A. Shrestha, S. R. Mohanty, S. K. Yadav, and P. N. Yadav, "Synthesis, Characterization, Anticancer, Pharmacokinetics and Molecular Docking Investigation of N (3)-alkyl Incorporated-3-acetyl-4-hydroxycoumarin Thiosemicarbazones and Their Copper (II) Complexes," *Journal of Molecular Structure* 1299 (2024): 136945.

66. D. F. Veber, S. R. Johnson, H. Y. Cheng, B. R. Smith, K. W. Ward, and K. D. Kopple, "Molecular Properties That Influence the Oral Bioavailability of Drug Candidates," *Journal of Medicinal Chemistry* 45 (2002): 2615–2623.

67. A. K. Ghose, V. N. Viswanadhan, and J. J. Wendoloski, "A Knowledge-Based Approach in Designing Combinatorial or Medicinal Chemistry Libraries for Drug Discovery. 1. A Qualitative and Quantitative Characterization of Known Drug Databases," *Journal of Combinatorial Chemistry* 1 (1999): 55–68.

68. I. Muegge, S. L. Heald, and D. Brittelli, "Simple Selection Criteria for Drug-Like Chemical Matter," *Journal of Medicinal Chemistry* 44 (2001): 1841–1846.

69. A. Daina and V. Zoete, "A BOILED Egg to Predict Gastrointestinal Absorption and Brain Penetration of Small Molecules," *ChemMedChem* 11 (2016): 1117–1121.

70. W. J. Egan, K. M. Merz, and J. J. Baldwin, "Prediction of Drug Absorption Using Multivariate Statistics," *Journal of Medicinal Chemistry* 43 (2000): 3867–3877.

71. S. Li, H. He, L. J. Parthiban, H. Yin, and A. T. M. Serajuddin, "IV-IVC Considerations in the Development of Immediate-Release Oral Dosage Form," *Journal of Pharmaceutical Sciences* 94 (2005): 1396–1417.

72. K. Palm, K. Luthman, A. L. Unge, G. Strandlund, and P. Artursson, "Correlation of Drug Absorption With Molecular Surface Properties," *Journal of Pharmaceutical Sciences* 85 (1996): 32–39.

73. P. K. Pandey, A. K. Sharma, and U. Gupta, "Blood Brain Barrier: An Overview on Strategies in Drug Delivery, Realistic In Vitro Modeling and In Vivo Live Tracking," *Tissue Barriers* 4 (2016): e1129476.

74. W. E. Evans and M. V. Relling, "Pharmacogenomics: Translating Functional Genomics Into Rational Therapeutics," *Science* 286 (1999): 487–491.

75. P. R. O. de Montellano, *Cytochrome P450: Structure, Mechanism, and Biochemistry* (Kluwer Acedemic/Plenum Publishers, 2005), 87–114.

76. W. Hamaguchi, N. Masuda, M. Isomura, et al., "Design and Synthesis of Novel Benzimidazole Derivatives as Phosphodiesterase 10A Inhibitors With Reduced CYP1A2 Inhibition," *Bioorganic & Medicinal Chemistry* 21, no. 24 (2013): 7612–7623, https://doi.org/10.1016/j.bmc.2013.10.035.

77. J. B. Baell and G. A. Holloway, "New Substructure Filters for Removal of Pan Assay Interference Compounds (Pains) From Screening Libraries and for Their Exclusion in Bioassays," *Journal of Medicinal Chemistry* 53 (2010): 2719–2740.

78. J. Baell and M. A. Walters, "Chemistry: Chemical Con Artists Foil Drug Discovery," *Nature* 513 (2014): 481–483.

79. R. Brenk, A. Schipani, D. James, et al., "Lessons Learnt From Assembling Screening Libraries for Drug Discovery for Neglected Diseases," *ChemMedChem* 3 (2008): 435–444.

80. S. J. Teague, A. M. Davis, P. D. Leeson, and T. Oprea, "The Design of Leadlike Combinatorial Libraries," *Angewandte Chemie International Edition* 38 (1999): 3743–3748.

81. P. Banerjee, A. O. Eckert, A. K. Schrey, and R. Preissner, "ProTox-II: A Webserver for the Prediction of Toxicity of Chemicals," *Nucleic Acids Research* 46 (2018): W257–W263.

82. P. Banerjee, F. O. Dehnbostel, and R. Preissner, "Prediction Is a Balancing Act: Importance of Sampling Methods to Balance Sensitivity and Specificity of Predictive Models Based on Imbalanced Chemical Data Sets," *Frontiers in Chemistry* 6 (2018): 362.

83. N. D. Malgorzata, P. Banerjee, M. Dunkel, R. W. Martin, and R. Preissner, "ProTox: A Web Server for the In Silico Prediction of Rodent Oral Toxicity," *Nucleic Acids Research* 42 (2014): 53–58.

Supporting Information

Additional supporting information can be found online in the Supporting Information section.

Figure S1: ^{1} H-NMR spectrum of *6-tert-butyl-4,8-dimethyl coumarin (3a)* ($C_{15}H_{18}O_2$). **Figure S2:** ^{13}C-NMR spectrum of *6-tert-butyl-4,8-dimethyl coumarin (3a)* ($C_{15}H_{18}O_2$). **Figure S3:** ^{1}H-NMR spectrum of *4,7,8-trimethyl coumarin (3b)* ($C_{12}H_{12}O_2$). **Figure S4:** ^{13}C-NMR spectrum of *4,7,8-trimethyl coumarin (3b)* ($C_{12}H_{12}O_2$). **Figure S5:** ^{1}H-NMR spectrum of *6-isopropyl-4-methyl coumarin (3c)* ($C_{13}H_{14}O_2$). **Figure S6:** ^{13} C-NMR spectrum of *6-isopropyl-4-methyl coumarin (3c)* ($C_{13}H_{14}O_2$).